HHS Public Access

Author manuscript

Nat Metab. Author manuscript; available in PMC 2023 March 06.

Published in final edited form as:

Nat Metab. 2021 September ; 3(9): 1189–1201. doi:10.1038/s42255-021-00454-z.

Umami-induced obesity and metabolic syndrome is mediated by nucleotide degradation and uric acid generation

Ana Andres-Hernando[1,2,6], **Christina Cicerchi**[1,6], **Masanari Kuwabara**[1], **David J. Orlicky**[3], **Laura Gabriela Sanchez-Lozada**[4], **Takahiko Nakagawa**[5], **Richard J. Johnson**[1], **Miguel A. Lanaspa**[1,2]

[1]Division of Renal Diseases and Hypertension, University of Colorado School of Medicine, Aurora, CO, USA.

[2]Division of Nephrology and Hypertension, Oregon Health Sciences University, Portland, OR, USA.

[3]Department of Pathology, University of Colorado School of Medicine, Aurora, CO, USA.

[4]Departamento de Fisiopatología Cardio-Renal, National Institute of Cardiology Ignacio Chavez, Tlalpan, México.

[5]Department of Nephrology, Rakuwakai Otowa Hospital, Kyoto, Japan.

[6]These authors contributed equally: Ana Andres-Hernando, Christina Cicerchi.

Abstract

Umami refers to the savoury taste that is mediated by monosodium glutamate (MSG) and enhanced by inosine monophosphate and other nucleotides. Umami foods have been suggested to increase the risk for obesity and metabolic syndrome but the mechanism is not understood. Here we show that MSG induces obesity, hypothalamic inflammation and central leptin resistance in male mice through the induction of AMP deaminase 2 and purine degradation. Mice lacking AMP deaminase 2 in both hepatocytes and neurons are protected from MSG-induced metabolic syndrome. This protection can be overcome by supplementation with inosine monophosphate, most probably owing to its degradation to uric acid as the effect can be blocked with allopurinol. Thus, umami foods induce obesity and metabolic syndrome by engaging the same purine

Correspondence and requests for materials should be addressed to Miguel A. Lanaspa. lanaspa@ohsu.edu.

Author contributions

M.A.L. and R.J.J. designed the research. M.A.L., A.A-H., L.G.S-L., T.N. and R.J.J. analysed the data. A.A-H., C.C., D.J.O., M.K. and M.A.L. performed the research. A.A-H., M.A.L. and R.J.J. wrote the paper.

Competing interests

M.A.L. and R.J.J. are inventors in two patents (nos. 13/814,568 and 62/473,005) related to the blockade of fructokinase to treat metabolic syndrome. M.A.L. and R.J.J. are founders and members of Colorado Research Partners, a company dedicated to the generation of fructokinase inhibitors. The other authors declare no competing interests.

Additional information

Extended data is available for this paper at https://doi.org/10.1038/s42255-021-00454-z.

Supplementary information The online version contains supplementary material available at https://doi.org/10.1038/s42255-021-00454-z.

Peer review information *Nature Metabolism* thanks the anonymous reviewers for their contribution to the peer review of this work. Christoph Schmitt was the primary handling editor.

nucleotide degradation pathway that is also activated by fructose and salt consumption. We suggest that the three tastes—sweet, salt and umami—developed to encourage food intake to facilitate energy storage and survival but drive obesity and diabetes in the setting of excess intake through similar mechanisms.

Of the five basic human tastes, human infants have an innate preference for sweet, salty and umami flavours, while showing an aversion to bitter and sour[1]. We hypothesize there may be an evolutionary basis for these preferences and that these tastes may have evolved to encourage the intake of specific foods that may aid survival in settings of food shortage. However, when intake is excessive, such as in modern society, their food-enhancing properties may be playing an important deleterious role in the development of obesity and diabetes.

For example, the major sweet foods available to our ancestors were fruits and honey, which are rich in fructose. We and others have shown that intake of fructose can preferentially increase energy stores by increasing visceral adiposity, inducing fatty liver and increasing serum triglycerides, while at the same time inducing insulin resistance, which preserves glucose for the brain by reducing its uptake in skeletal muscle[2–5]. Indeed, many species appear to utilize fructose as a means for increasing energy stores, including long distance migrating birds, fruit-eating fish such as the Pacu and even the great apes[6]. Today, however, the intake of added sugars containing fructose, such as high-fructose corn syrup and sucrose, has led to such large intakes that it has received central attention as one of the drivers of metabolic syndrome[7].

High-salt diets have also been epidemiologically linked with obesity and metabolic syndrome[8–10] and our group was able to show that the mechanism involves a rise in serum osmolality with the induction of aldose reductase, which induces fructose production in the liver and brain[11]. Indeed, we found that high-salt diets also result in obesity and metabolic syndrome in mice, although the process is slower than with dietary fructose. Importantly, blocking fructose metabolism blocks high-salt diet-induced metabolic syndrome and blood pressure changes[11].

The mechanism by which fructose induces metabolic syndrome has been shown to be due to the rapid metabolism of fructose to fructose-1-phosphate by ketohexokinase-C (KHK-C). Fructose metabolism through KHK-C causes a transient decrease in intracellular phosphate and ATP that activates the enzyme AMP deaminase-2 (AMPD2). In turn, AMPD2 converts AMP to inosine monophosphate (IMP) that then eventually degrades to hypoxanthine and uric acid. We have shown that this nucleotide degradation pathway has a key role in driving the metabolic syndrome and that it is mediated by mitochondrial oxidative stress and inhibition of AMP-activated protein kinase that maintains low intracellular ATP levels[12–14].

Umami is the ‘savoury’ taste and is due to the presence of free glutamate that is released during ripening, ageing, drying, curing or cooking of foods. MSG is also commonly added to foods to enhance taste. Of interest, uptake of glutamate in the liver results in conversion to glutamine and the generation of nucleotides[15] that can be degraded to uric acid, suggesting a link with fructose metabolism. Furthermore, the flavour of umami can be enhanced by

IMP, AMP and guanosine monophosphate (GMP) in foods due to their ability to enhance glutamate binding to the umami receptor in the taste buds of the tongue[16]. Umami foods are also characteristically the same foods that increase the risk for gout[17] and the enzyme AMPD has been considered a key enzyme involved in the generation of umami foods[18].

Thus, we hypothesized, that umami foods might be able to bypass the fructose pathway to directly stimulate the development of obesity and metabolic syndrome. Indeed, there are reports that the intake of umami foods can increase the risk for developing obesity[19,20]. Some studies have also reported that the intake of MSG can induce obesity in animals, especially young mice[21,22], while others have challenged this finding[23,24]. Importantly, no studies have investigated the interaction with nucleosides such as IMP and none have investigated the role of the purine degradation pathway.

Results

MSG promotes caloric intake and metabolic syndrome in mice.

MSG increases food intake and causes weight gain.—To test the effects of MSG on caloric intake, we first analysed the response of adult wild-type (WT) mice to increasing concentrations of MSG, from 60 to 300 mM (1–5% w/v) in drinking water for 2 weeks. No adverse reactions or visual behavioural changes (such as dominance, activity or fighting) were observed in any of the groups analysed. As shown in Fig. 1a,b, MSG increased both water and chow intake in a dose-dependent manner. Compared to water control, concentrations of 60 and 300 mM of MSG resulted in increases of daily caloric intake of 19.6 and 24.8%, respectively ($P < 0.01$). As a result of increased caloric intake, body weight gains were elevated in MSG-exposed mice compared to controls on water alone. During the first 2 weeks, mice on 60 and 300 mM of MSG solutions gained an average of 3.2 (12.8%) and 4.8 (19.2%) grams compared to a weight gain of 0.9 (3.6%) grams in water-treated controls ($P < 0.01$).

AMPD2 drives both MSG-mediated preference and food intake.

The metabolism of glutamate in the liver involves its conversion to glutamine, which then enters into the purine synthesis pathway to generate IMP and other purine nucleotides with substantial cellular energy (ATP) consumption[15]. Consistently, intrahepatic levels of uric acid, a product derived from IMP and nucleotide turnover were increased in MSG-exposed mice in parallel with significantly lower levels of ATP (Fig. 1c,d) and activation of AMPD, the first enzyme involved in the purine degradation pathway (Fig. 1e,f). Therefore, to determine if the activation of the main AMPD isoform, AMPD2, and the purine degradation pathway regulated MSG-dependent food intake, we next evaluated the preference and caloric intake in response to MSG of whole-body AMPD2 knockout mice compared to that of weight-matched (23.4 ± 0.5 versus 23.7 ± 0.8, P = not significant (NS)) WT mice (Fig. 1g–i). As shown in Fig. 1h, compared to WT animals, global AMPD2 knockout mice demonstrated significantly reduced preference for 300 mM of MSG than WT mice in 2-bottle choice paradigms. While WT mice preferred MSG over water solutions (69.14% preference at 300 mM of MSG), no substantial preference over water was observed in AMPD2 knockout mice (47.02% 300 mM of MSG versus 52.98% of water).

Furthermore, water intake was not elevated in AMPD2 knockout mice (Fig. 1i); importantly, no increased food intake was observed compared to WT animals (Fig. 1j). Consistent with these observations, intrahepatic uric acid levels were significantly lower in global AMPD2 knockout mice on MSG in parallel with markedly higher ATP levels (Fig. 1j–l).

Neuronal AMPD2 in mediates MSG preference and food intake.

The observation that global AMPD2 knockout mice lost their preference for glutamate and that this prevented the increased caloric intake raised the question of whether neuronal AMPD2 might be responsible. Neuron-specific AMPD2 knockout mice were generated using a Cre-synapsin mouse (Fig. 2a,b). Like the global AMPD2 knockout, the neuron-specific AMPD2 knockout mouse showed nearly absent preference of mice for MSG with no increase in total caloric intake (Fig. 2c–g) compared to weight-matched AMPD2$^{loxP/loxP}$ controls (24.2 ± 0.6 versus 23.9 ± 0.3, P = NS). Similarly, whereas MSG-treated AMPD2$^{loxP/loxP}$ mouse had increased uric acid and decreased ATP content in the hypothalamus, this was prevented in the neuron-specific AMPD2 knockout (Fig. 2h,i).

Like fructose, MSG promotes metabolic syndrome.

To test whether the observed increased caloric intake induced by MSG could induce metabolic syndrome in mice, we exposed WT mice to 300 mM of MSG for 15 weeks and compared their metabolic response with that of weight-matched mice exposed to the same amounts of fructose (300 mM or 5% w/v). In this regard, we previously showed that 15% w/v fructose solutions induce metabolic syndrome in WT mice in 25 weeks[4]. As shown in Extended Data Fig. 1a, the intake of fructose and MSG was significantly higher than regular water control, although mice on fructose drank slightly more than mice on MSG (6.83 ± 0.4 ml of fructose per day versus 6.14 ± 0.4 ml of MSG per day, $P < 0.01$).

We previously reported that chronic fructose intake of mice leads to excessive food intake but this increased energy intake does not occur until after several months. Indeed, in the first few months fructose-fed mice decreased their chow intake in response to the caloric load of fructose. By contrast, while MSG also confers 4 cal g^{-1}, mice on MSG did not demonstrate reduced chow intake but they responded by consuming more chow than control (water) or fructose-fed mice (3.68 ± 0.2 g chow per day versus 2.93 ± 0.2 and 2.71 ± 0.1 g in water and fructose-fed mice, respectively, $P < 0.01$; Extended Data Fig. 1b). Consequently, over the 15 weeks, the total caloric intake in MSG-fed mice was markedly higher (1,324 ± 34 cal versus 966 ± 31 and 1,086 ± 49 cal in water and fructose-fed mice, respectively, $P < 0.01$; Extended Data Fig. 1c). As shown in Extended Data Fig. 1d–m, mice on MSG also gained significantly more weight, which was paralleled by increased liver and epididymal adipose weights, liver fat content and adipose inflammation as well as markedly higher levels of plasma aspartate aminotransferase (AST), a marker of liver inflammation, insulin and leptin.

MSG-induced metabolic syndrome depends on hepatic AMPD2.

The observation that the preference for MSG was dependent on AMPD2 activity in the brain made us realize that to test if AMPD2 mediates the metabolic syndrome, we would need to assure similar intake of MSG in WT and AMPD2 knockout mice. In studies with fructose, we previously identified the liver as the primary site driving the metabolic syndrome[25].

Therefore, we decided to evaluate whether knocking out AMPD2 in the liver would result in continued preference for MSG so that similar intakes could be achieved. As shown in Fig. 3, we knocked down hepatocyte AMPD2 by crossing with a Cre-albumin mouse (Fig. 3a); the residual AMPD2 might be from other resident, for example, Ito cell populations in the liver. Importantly, liver-specific AMPD2 knockout also showed reduced preference for MSG with decreased caloric intake similar to the global AMPD2 knockout (Fig. 3b,c). To perform a study with equal intake between AMPD2$^{loxP/loxP}$ control mice and liver-specific AMPD2 knockout mice, we administered 300 mM of MSG to liver-specific knockout and 200 mM of MSG to weight-matched (24.3 ± 0.6 versus 24.1 ± 0.4, P = NS) WT mice, which resulted in comparable intakes (Fig. 3d). Importantly, hepatocyte-specific AMPD2 knockout mice were fully protected from metabolic syndrome compared to the AMPD2$^{loxP/loxP}$ control mice when evaluated after 15 weeks (Fig. 3e–k).

Reducing AMPD2 can treat MSG-induced metabolic syndrome.

The observation that metabolic syndrome from MSG could be prevented in the AMPD2 knockout model also raised the question of whether it might be a new therapeutic target. To study this, we decided to knockdown AMPD2 in adult mice who already had features of metabolic syndrome from MSG intake. Specifically, we generated tamoxifen-dependent inducible AMPD2 knockout mice. As shown in Fig. 4a,b, administration of tamoxifen in mice pre-exposed to MSG for 7 weeks resulted in the deletion of AMPD2 expression in both the liver and hypothalamus in as early as 5 d post-treatment. Consistently and compared to vehicle-treated uninduced AMPD2 knockout (AMPD2$^{loxP/loxP}$ × Cre-ubiquitin-conjugating enzyme (UBC)) control mice, both MSG and total caloric intakes significantly decreased as early as 3 d after tamoxifen treatment (Fig. 4c,d) resulting in a marked reduction of body weight gain, adiposity and metabolic dysfunction (Fig. 4e–j). Similar results were found when we analysed the response to tamoxifen of control non-inducible AMPD2$^{loxP/loxP}$ mice versus AMPD2$^{loxP/loxP}$ × Cre-UBC (Extended Data Fig. 2). As shown in the figure and unlike inducible AMPD2$^{loxP/loxP}$ × Cre-UBC, tamoxifen treatment did not reduce the progression of metabolic syndrome and leptin resistance in AMPD2$^{loxP/loxP}$ animals indicating that the beneficial effects observed by deleting AMPD2 expression in mice were not due to tamoxifen administration.

IMP exacerbates the metabolic effects of MSG.

Besides being the immediate product of AMPD2 in the purine nucleotide synthesis pathway from glutamate/glutamine metabolism (Fig. 1e), IMP is a known taste enhancer of MSG[26]. In this regard, addition of 500 μM of IMP significantly increases the preference score of humans for MSG without altering the detection threshold[27]. Intrigued by these, we characterized the metabolic effects of MSG + IMP combinations compared to MSG alone. To this end, we exposed WT and AMPD2 knockout mice to 30 mM of MSG alone or in combination with 300 μM of IMP. We selected a 30-mM MSG concentration based on our data in Fig. 1b demonstrating that, at this concentration, MSG does not acutely promote increased caloric intake.

Effect of IMP on preference and intake in MSG-treated mice.

We first performed a two-bottle preference test to determine if IMP enhanced the intake of low MSG levels (30 mM) in WT and AMPD knockout mice (average over 7 days; Fig. 5a,g,j). The main finding was that IMP increased the preference for MSG in both WT and AMPD2 knockout mice compared to MSG or IMP alone. This effect was paralleled by a marked increase in AMPD activity by MSG + IMP in both the liver and hypothalamus of mice (Fig. 5d,e). Of interest, activation of AMPD was not necessarily associated with higher AMPD2 expression in the liver or hypothalamus (Fig. 5f). We next provided WT and AMPD2-deficient mice with MSG, IMP or the combination in a single-bottle study over 7 d. While IMP alone increased food intake slightly, the combination of MSG and IMP resulted in significantly higher water and food intake in WT mice on MSG + IMP compared to water or mice exposed to either MSG or IMP alone (Fig. 5b,c). However, while a similar enhancement of IMP on MSG preference and intake was observed in AMPD2 knockout mice (Fig. 5g–k), the increase in food intake was significantly less than that observed in WT mice receiving MSG and IMP (Fig. 5l).These data suggest that while IMP has a modest ability to stimulate food intake on its own as observed in Fig. 5c,i, it has a more marked effect on enhancing the preference for MSG and thus stimulating MSG-dependent caloric intake, particularly in WT mice.

IMP accelerates MSG-induced metabolic syndrome.

Since IMP markedly potentiates caloric intake in MSG-exposed mice, we then examined whether chronic MSG + IMP feeding could exacerbate metabolic syndrome compared to mice given MSG alone. To this end, WT mice were exposed to regular water control, 30 mM of MSG, 300 μM of IMP or a combination of MSG + IMP and the features of metabolic syndrome were characterized for 30 weeks. As expected and as shown in Fig. 6a and Supplementary Table 1, the combination of MSG + IMP markedly stimulated body weight gain. At the end of the 30 weeks, mice on MSG + IMP gained over 22 g on average with final body weights of 46.4 ± 2.2 g, which were significantly higher than water controls. Of interest, mice on MSG or IMP alone also gained more weight than water controls (14.5 and 15.2 g on average, respectively). As shown in Fig. 6, increased body weight in MSG + IMP-receiving mice correlated with greater epididymal adipose (Fig. 6b) weight and inflammation as demonstrated in H&E stained sections (Fig. 6c) and by crown structure (inflammatory foci) scoring (Fig. 6d). We also found significant liver steatosis in mice on MSG + IMP, which was characterized by increased liver weights, large areas of macro- and microsteatosis in H&E stained sections, and elevated intrahepatic triglyceride content and plasma AST levels (Fig. 6e–h). Furthermore, mice on MSG + IMP developed insulin resistance, characterized by increased fasting insulin, glucose and homoeostasis model assessment-insulin resistance (Fig. 6i and Supplementary Table 1) and validated by both oral glucose (OGTTs) and insulin tolerance tests (ITTs) (Fig. 6j–m and Supplementary Table 1).

Early leptin resistance is induced by MSG and IMP in mice.

The observation of increased caloric intake with MSG raised the possibility that this might be due to leptin resistance. To this end, we exposed weight-matched WT mice to water,

MSG, IMP or a combination of MSG + IMP. As shown in Fig. 7a and Supplementary Table 1, the accumulated caloric intake in mice on MSG + IMP over the 30 weeks was markedly higher than the rest of the groups (3,321 ± 198 cal versus 2,057 ± 102, 2,309 ± 62 and 2,512 ± 112 in water, MSG and IMP groups, respectively $P < 0.01$). In parallel with increased caloric intake, leptin levels both in plasma and adipose tissue were significantly higher in MSG + IMP-receiving mice (Fig. 7b,c and Supplementary Table 1), which is suggestive of reduced leptin sensitivity or leptin resistance. Of interest, both increased body weight and plasma leptin levels were apparent as early as 1 week from exposure to MSG + IMP and most notable from week 2 (Fig. 7d,e). This would indicate that a marked reduced leptin sensitivity from MSG + IMP should be observed at a very early time point. To test for leptin sensitivity, we administered leptin (1 μg g^{-1} intraperitoneally) and observed the effect on phosphorylated STAT3 levels in the hypothalamus (a sign of leptin signalling) and subsequent food intake[28]. Unlike control mice or mice on MSG or IMP only, animals fed MSG + IMP showed reduced phosphorylated STAT3 as early as two weeks after the start of treatment, which is suggestive of leptin resistance, and also did not suppress their food intake (Fig. 7f,g). Central leptin resistance is associated with hypothalamic inflammation and oxidative stress. Of interest, the reduced leptin sensitivity observed in MSG + IMP-exposed mice correlated with significantly higher levels of hypothalamic uric acid (Fig. 7h). In this regard, we and others have previously shown that even though uric acid can act as an antioxidant molecule, intracellularly it is a potent pro-oxidant[13,29]. Consistent with higher uric acid, the hypothalamic levels of thiobarbituric acid (TBARS) as well as messenger RNA expression of pro-inflammatory cytokines (IL-6 and TNF) were elevated in MSG + IMP-fed mice compared to the rest of the groups (Fig. 7h–j). Furthermore, hypothalamic expression of the leptin receptor (LEPR) was also upregulated in MSG + IMP-exposed mice (Fig. 7j). Similar findings were observed over time for up to 30 weeks (Extended Data Fig. 3).

We also evaluated the response of weight-matched animals to leptin as early as 3 d after exposure to MSG + IMP (Fig. 7k–o). Over the 3-d period, no substantial changes were observed in body weight gain or plasma leptin levels (Fig. 7k,l). However, food intake was not suppressed after leptin injection in WT mice receiving MSG + IMP and this was associated with increased hypothalamic levels of uric acid and TBARS (Fig. 7m–o). The observation that resistance to leptin by MSG + IMP preceded the onset of hyperleptinaemia and also occurred when mice were phenotypically lean suggests that leptin resistance was induced early by MSG + IMP; however, it is possible that hedonic or other behavioural responses might also mimic some of these effects.

MSG and IMP act via both hepatic and hypothalamic AMPD2.

We also determined whether leptin resistance was mediated by neuronal or hepatic AMPD2. As shown in Fig. 7p, the blockade of AMPD2 in the liver or brain markedly improved the sensitivity to leptin in mice exposed to 300 mM of MSG, which was markedly reversed when IMP was added back (Fig. 7q).

Uric acid mediates MSG + IMP-dependent metabolic syndrome.

As we indicated previously, IMP can act both as a taste enhancer for MSG and as a metabolite produced from glutamate in the purine nucleotide pathway. To further elucidate

whether the molecular mechanism whereby IMP potentiates the deleterious effects of MSG on metabolic syndrome are mediated by its metabolism, we tested the effects of downstream products of IMP on MSG-induced metabolic syndrome in mice. All metabolites were tested at the same concentration (300 μM). As shown in Extended Data Fig. 4a,b, besides IMP, other products from IMP metabolism including inosine, hypoxanthine and uric acid caused both increased caloric intake and weight gain, even in the absence of MSG. Of interest, allantoin, which is produced enzymatically from uric acid in most mammals but not in humans, failed to induce any deleterious effects in WT mice. This would suggest that the accumulation of uric acid is an important deleterious step in MSG + IMP-dependent metabolic syndrome.

To test this hypothesis, we next examined the metabolic response of WT mice exposed to combinations of MSG with different products of the purine degradation pathway for 30 weeks. As shown in Extended Data Fig. 4c,d and Supplementary Table 1, besides IMP, the addition of inosine, hypoxanthine and uric acid but not allantoin stimulated both body weight gain and caloric intake in association with a marked reduction in hepatic ATP content (Supplementary Table 1). Mice exposed to these purines in combination with MSG demonstrated greater adipose and liver weights (Extended Data Fig. 4e,f). Enlarged livers correlated with greater hepatic steatosis and liver injury as denoted both in haematoxylin and eosin (H&E) histological sections as well as by the determination of intrahepatic triglycerides and plasma AST (Extended Data Fig. 4g–i and Supplementary Table 1). Similarly, both hyperinsulinaemia and hyperleptinaemia were found in mice fed combinations of MSG and IMP, inosine, hypoxanthine and uric acid (Extended Data Fig. 4j,k and Supplementary Table 1).

Uric acid mediates IMP effects on metabolic syndrome.

As shown in both Extended Data Fig. 4c–k and Supplementary Table 1, a differential metabolic response of mice to the multiple products of the purine degradation pathway from IMP was observed, with animals on MSG + uric acid developing the most severe phenotype. This observation and the failure of MSG + allantoin in inducing metabolic syndrome in mice would suggest that blockade of uric acid accumulation could prevent metabolic syndrome induced by MSG + IMP. To evaluate this possibility, we exposed WT mice to MSG + IMP alone or in combination with a xanthine oxidase inhibitor, allopurinol (1.1 mM), for 30 weeks to block the production of uric acid. As shown in Extended Data Fig. 5a,b, allopurinol markedly reduced both plasma and intrahepatic uric acid levels compared to untreated mice receiving MSG + IMP. Of interest, cumulative caloric intake as well as body weight gain were markedly reduced in MSG + IMP + allopurinol-fed mice (Extended Data Fig. 5c,d). The reduction in body weight in these mice compared to MSG + IMP-fed animals correlated with reduced adipose and liver weights, liver steatosis and injury and plasma levels of insulin and leptin (Extended Data Fig. 5e–j).

Discussion

Umami (or ‘savoury’) mediated by glutamate is one of the five major tastes and is preferred even by infants, thus suggesting an innate preference[1]. In this study, we showed that MSG

both activates and provides fuel for the nucleotide degradation pathway, which is similarly activated by fructose and high-salt diets. Like these other diets, MSG stimulates weight gain and induces mild features of metabolic syndrome. However, when MSG is combined with IMP, the effects on inducing metabolic syndrome are dramatically enhanced. Indeed, other components of the nucleotide degradation pathway, such as inosine, hypoxanthine and uric acid, can also enhance the metabolic effects of glutamate; importantly, these effects appear to be mediated by uric acid. Thus, these studies support the hypothesis that the three desired tastes (sweet, salt and umami) may have developed to encourage the intake of foods that have the ability to aid the storage of fuel and prepare an animal for periods of food shortage[30].

One of the first major findings was that glutamate activated AMPD2 in the liver and brain. AMPD2 is an important enzyme that counteracts the effects of AMP-activated protein kinase, thus favouring the production of lipids and glycogen and the development of insulin resistance[12,31]. Indeed, we showed that both the preference for MSG and the effect of MSG in increasing caloric intake by inducing leptin resistance was observed in hepatocyte- and neuron-specific AMPD2 knockout mice, suggesting a key role for AMPD2 in these tissues in driving MSG effects (Figs. 2 and 3). Of note, even though AMPD2 knockout mice showed a tendency to consume lower calories, no significant differences were observed in baseline food intake between WT and AMPD2 knockout mice (3.06 ± 0.19 versus 2.84 ± 0.14 g, $n = 6$, $P = 0.064$) or between control AMPD2$^{loxP/loxP}$ mice and liver- (3.16 ± 0.10 versus 3.18 ± 0.11 g, $n = 6$; $P = 0.74$) or neuron-specific AMPD2 knockout (3.16 ± 0.10 versus 3.08 ± 0.10 g, $n = 6$, $P = 0.19$) mice. It is also important to note that in the brain, the action of AMPD2 to regulate intake may be relevant in other cell types besides neurons. In this regard, we found that chronic (15-week) exposure to IMP and MSG + IMP results in a marked increase in the hypothalamic expression of GFAP and IBA1, specific markers of astrocytes and microglia, respectively (Extended Data Fig. 6).

One of the mechanisms by which AMPD2 mediates its metabolic effects is by the downstream breakdown of IMP to uric acid, which acts to inhibit AMP-activated protein kinase and stimulate mitochondrial oxidative stress that impairs fatty acid oxidation and stimulates lipogenesis[12–14]. Interestingly, while IMP acts to enhance glutamate binding to the umami receptor in the tongue, the ingestion of IMP also rapidly increases serum uric acid in humans[32]. Indeed, RNA is also converted to purine nucleotides by pancreatic ribonucleases in the gut, which are then degraded by phosphatases in the small intestinal villi, followed by uptake into enterocytes where they are degraded to uric acid. Thus, the ingestion of IMP facilitates the generation of uric acid. In this regard, it is important to note that the study by Lu et al.[33] demonstrated a critical role for uric acid in inducing hypothalamic inflammation. Even though we have not tested directly whether hypothalamic uric acid reduced central leptin sensitivity and thus stimulated caloric intake, our studies demonstrate that blockade of uric acid production with allopurinol markedly ameliorated both caloric intake and metabolic dysfunction and specific deletion of AMPD2 in neurons resulted in lower hypothalamic uric acid and a substantial reduction in total caloric intake and in the preference of mice for MSG.

To address the role of uric acid in the mechanism by which IMP exacerbates glutamate-induced metabolic syndrome, we first showed that substitution of IMP with inosine, hypoxanthine and uric acid resulted in similar metabolic effects, whereas substitution with allantoin (a product downstream of uric acid that lacks the purine ring) had no effect. We also showed that administration of allopurinol, a xanthine oxidase inhibitor that blocks uric acid formation in response to IMP, protected the animals from MSG-induced metabolic syndrome.

While our studies document that umami foods can induce metabolic syndrome in animals, the importance of MSG and the umami pathway for human obesity and diabetes can be debated. Currently, intake of free glutamate is approximately 500–550 mg per day in the UK, while intake is typically 1.2–1.7 g d^{-1} in Japan[19]. Some individuals can ingest up to 10 g of MSG in a day. In our studies, we found that the dose of glutamate necessary to induce metabolic syndrome was greater than 60 mM or 1% w/v. However, it is more important to better understand how much IMP or related nucleotides are being administered and whether the effects of umami foods are enhanced in the setting of hyperuricaemia. Indeed, we previously reported that high uric acid levels can act to enhance the ability to induce metabolic syndrome by stimulating upstream pathways such as aldose reductase[34] and fructokinase[35]. Thus, it is possible that a hyperuricaemia might enhance the ability of umami foods to cause obesity and diabetes.

Our study has some limitations. First, the study was carried out in mice and general translation to human disease will require additional studies. Second, some renal toxicity with elevated plasma creatinine and blood urea nitrogen occurred when MSG was given over 30 weeks with IMP and especially with inosine and uric acid (Supplementary Table 1), probably from the effects of uric acid. However, renal disease would have been expected to reduce and not stimulate weight gain. Also, several studies have demonstrated the importance of AMPD isoforms and particularly AMPD2 in brain development. However, while AMPD2 deficiency has been associated with neurodevelopmental issues in humans, similar findings are observed in mice only when both AMPD2 and AMPD3 are deleted. This redundancy may have protected AMPD2 knockout mice from any neurodevelopmental issues. The protection observed in liver-specific AMPD2 knockout mice would indicate that the beneficial effects of blocking AMPD2 are independent of any neurodevelopmental issues. Consistently, and using an inducible model, we have provided evidence that targeting AMPD2 would be beneficial against metabolic syndrome in fully developed adult mice. An additional limitation is that we could not exclude the possibility that small differences in baseline food intake could contribute to phenotype, despite our overall data supporting a significant role for MSG-induced leptin resistance. Another limitation of our study is that we could not conclude that the beneficial effect against MSG-induced metabolic dysfunction by blocking xanthine oxidase is necessarily mediated by uric acid or rather by the accumulation of upstream products (e.g. inosine, hypoxanthine, xanthine), which would exert potential beneficial effects. Even though our data in Fig. 8 suggest a deleterious effect of these purine metabolites, the use of ‘humanized’ uricase knockout mice, which would have greater uric acid levels, would be particularly informative. Also, future studies with the addition of uric acid in allopurinol-treated mice would need to be carried out to tease out the specific role of uric acid in MSG-induced metabolic dysfunction.

In summary, our results support the hypothesis depicted in Fig. 8 where the addition of IMP and downstream products including inosine, hypoxanthine and uric acid to MSG markedly exacerbated the effects of glutamate to increase caloric intake and induce metabolic syndrome. Excessive glutamate appears to act both by stimulating purine nucleotide production, lowering ATP levels and activating AMPD2. IMP formed from both glutamine and resulting from AMPD2 activation enters the purine degradation pathway to generate uric acid, resulting in oxidative stress and inflammation. Depleted ATP coupled with uric acid-dependent oxidative and inflammatory conditions stimulate fat accumulation in the liver and adipose tissue and decrease the sensitivity of the hypothalamus to leptin, which further promotes food and caloric intake. Thus, we suggest that umami foods, like salt and sugar, may all engage a similar survival pathway that was utilized by ancestral humans for survival but increase our risk for metabolic diseases today.

Methods

Animals and reagents.

AMPD2 knockout mice (B6.129-*Ampd2*^{tm1Tm}/J) were originally obtained from the Jackson Laboratory and a colony is maintained at the University of Colorado. On reception, mice were bred with pure C57BL/6 mice to obtain both knockout and WT littermates. All experimental mice were maintained in temperature- and humidity-controlled specific pathogen-free condition on a 14-h dark/10-h light cycle and allowed ad libitum access to normal laboratory chow (catalogue no. 2920X; Harlan Teklad). Conditional AMPD2 knockout mice were developed by Ingenious Targeting Laboratory using the Cre-Lox system. To this end, exons 2–9 were flanked by *loxP* sites for Cre recombinase-specific deletion. Tissue specific Cre-expressing mice were purchased from the Jackson Laboratory —Cre-albumin (stock no. 018961) for silencing AMPD2 in hepatocytes and Cre-synapsin (stock no. 003966). Similarly, tamoxifen-dependent inducible AMPD2 knockout mice were made by crossing these mice with mice expressing tamoxifen-inducible Cre recombinase under the ubiquitin gene (stock no. 008085). Tamoxifen was provided intraperitoneally at a dose of 75 mg kg^{-1} for 5 consecutive days. All experiments were conducted with adherence to the National Institutes of Health (NIH) Guide for the Care and Use of Laboratory Animals[36]. In all studies, 7–10-week-old male mice with non-significant differences in baseline body weights were employed. For all studies, baseline body weights were in the range of 23.9 ± 0.7 g. Water and food consumption was monitored daily and body weight recorded weekly for 30 weeks. Caloric intake was calculated as the sum of chow intake (3.1 cal g^{-1}) and water intake (accounting for the fact that fructose, glucose and glutamate provide 4 cal g^{-1}). For the two-bottle preference studies, mice were housed individually and provided with two similar water bottles filled with water for acclimation for a 5-d period. For the experiment, water in one of the bottles was substituted with water containing MSG, IMP or a mixture of MSG + IMP. One day after exposure, the position of the two bottles was switched to control for side preference. The preference ratio was calculated as the ratio of volume of tastant consumed over the 2-d test period to total volume consumed, that is, a score of 0.5 or 50% shows no preference. Total fat mass and percentage of fat/fat-free mass was analysed by EchoMRI as described previously[25].

All consumable reagents (MSG, IMP, inosine, hypoxanthine, uric acid, fructose and glucose) were obtained from Sigma-Aldrich. Similarly, mouse leptin was purchased from Sigma-Aldrich (catalogue no. L3772) and insulin was obtained from Eli Lilly (Humulin). The animal protocol was approved by the Institutional Animal Care and Use Committee of the University of Colorado.

Biochemical analysis.

Blood was collected in microtainer tubes (BD) from cardiac puncture of mice under isoflurane; serum was obtained after centrifugation at 13,600 *g* for 2 min at room temperature. Serum parameters were performed biochemically according to the manufacturer's instruction (uric acid: catalogue no. DIUA-250, Bioassay systems; AST: catalogue no. EASTR-100, Bioassay Systems; ALT: catalogue no. EALT-100, Bioassay Systems; insulin: catalogue no. 90080, Crystal Chem; leptin: catalogue no. MOB00, R&D Systems). Determination of parameters in tissue was performed in freeze-clamped tissues and measured biochemically according to the manufacturer's protocol (triglycerides (liver): catalogue no. ETGA-200, Bioassay Systems; uric acid: catalogue no. DIUA-250, Bioassay Systems; ATP: catalogue no. EATP-100, Bioassay Systems).

AMPD activity was analysed by measuring the amount of ammonia released in response to AMP as described previously[37]. Briefly, fresh liver extracts (50 mg) were collected in a buffer containing 150 mM of KCl, 20 mM of Tris-HCl, pH 7.5, 1 mM of EDTA and 1 mM of dithiothreitol. The reaction mixture consisted of 25 mM of sodium citrate, pH 6.0, 50 mM of potassium chloride and varying concentrations of AMP. The enzyme reaction was initiated by the addition of the enzyme solution and incubated at 37 °C for 15 min for all samples collected. The reactions were stopped by adding the phenol/hypochlorite reagents: reagent A (100 mM of phenol and 0.050 g l^{-1} sodium nitroprusside in water) was added, followed by reagent B (125 mM of sodium hydroxide, 200 mM of dibasic sodium phosphate and 0.1% sodium hypochlorite in H_2O). After incubation for 30 min at 25 °C, the absorbance of the samples was measured at 625 nm with a spectrophotometer. To determine the absolute specific activity of ammonia production (μmol ammonia per minute), a calibration curve was determined in the range of 5 μM to 1 mM of ammonia.

Sample collection.

For tissue collection, mice were anaesthetized with 1–3% isoflurane via a nose cone and tissues were quickly dissected and snap-frozen (<5 s) in liquid nitrogen with a precooled Wollenberger clamp. To eliminate the potential effect of heterogeneity across different lobes of the liver, the whole liver was collected and grounded. For hypothalamic collection, the brain was positioned with the ventral surface up and the hypothalamic area microdissected and snap-frozen in liquid nitrogen using the optic chiasm and optic tracts as landmarks.

Histopathology.

Formalin-fixed paraffin-embedded liver and epididymal adipose sections were stained with H&E. Histological examination was performed through an entire cross-section of liver from each mouse. Crown structures were scored as follows: <3 per 40× field = 0; 3–10 per 40× field = 1; 11–25 per 40× field = 2; and >25 crown structures per 40× field = 3. The

entire cross-section of epididymal adipose tissue was scored for each animal and averages were arrived at for each animal. Images were captured on an Olympus BX51 microscope equipped with a 4 MP MacroFire digital camera (Optronics) using the PictureFrame application v.2.3 (Optronics). Composite images were assembled with the use of Adobe Photoshop 2021. All images in each composite were handled identically.

Western blotting.

Protein lysates were prepared from mouse tissues using MAP kinase lysis buffer as described previously[38]. Protein content was determined using the bicinchoninic acid protein assay (Pierce). Total protein (40 μg in liver and 25 μg in hypothalamic samples) was separated by SDS–polyacrylamide gel electrophoresis (10% w/v) and transferred to polyvinylidene fluoride membranes (Bio-Rad Laboratories). Membranes were first blocked for 1 h at 25 °C in 4% (w/v) instant milk dissolved in 0.1% Tween 20 Tris-buffered saline, incubated with primary rabbit or mouse-raised antibodies (1:1,000 dilution in Tween 20 Tris-buffered saline) pSTAT3/STAT3 (catalogue no. 12640S, Cell Signaling Technology; research resource identifier (RRID): AB_2629499, AB_331586), AMPD2 (Abnova 271, RRID: AB_1236647) and actin (catalogue no. 4968S, Cell Signaling Technology; RRID: 2313904) and visualized using an anti-rabbit (catalogue no. 7074; RRID: AB_2099233) or anti-mouse IgG (catalogue no. 7076; RRID:AB_330924) horseradish peroxidase-conjugated secondary antibody (1:2,000, Cell Signaling Technology) using the HRP Immunstar detection kit (Bio-Rad Laboratories). Chemiluminescence was recorded with an Image Station 440 CF and results were analysed with the 1D Image software version 3.6 (Kodak Digital Science).

Leptin and ITTs.

Insulin sensitivity was determined by both OGTTs and ITTs as described previously[11]. For leptin sensitivity, mice were habituated to injection by receiving intraperitoneal saline on fasting condition for three consecutive days. At day four, food was removed and animals were injected with either saline (control) or leptin (0.6 mg kg^{-1} body weight; PeproTech) and the amount of food consumed afterwards was recorded for 7 h. For hypothalamic activation of STAT3, mice were injected with leptin and killed 1 h postinjection. The hypothalamic area of the brain was the dissected out and lysed and the total and phosphorylated (S727) STAT3 levels analysed by western blot.

Statistical analysis.

All numerical data are presented as the mean ± s.e.m. Independent replicates for each data point (*n*) are identified in the figure legends. Data graphics and statistical analysis were performed using Prism 5 (GraphPad Software). Data without indications were analysed by one-way analysis of variance (ANOVA) and Tukey's posthoc test. $P < 0.05$ was regarded as statistically significant. Animals were randomly allocated in each group using Research Randomizer (www.randomizer.org). No animals were excluded from the study.

Reporting Summary.

Further information on research design is available in the Nature Research Reporting Summary linked to this article.

Data availability

Requests for resources, newly generated mouse lines and reagents should be directed to and will be fulfilled by the lead contact, M.A.L. Figures 1–7 and Extended Data Figs. 1–6 represent in their majority the raw data from all individual points. The data that support the findings of this study are available from the corresponding author on reasonable request. This study did not generate unique datasets or code. Raw individual datasets for each study and figures will be available on reasonable request. Source data are provided with this paper.

Extended Data

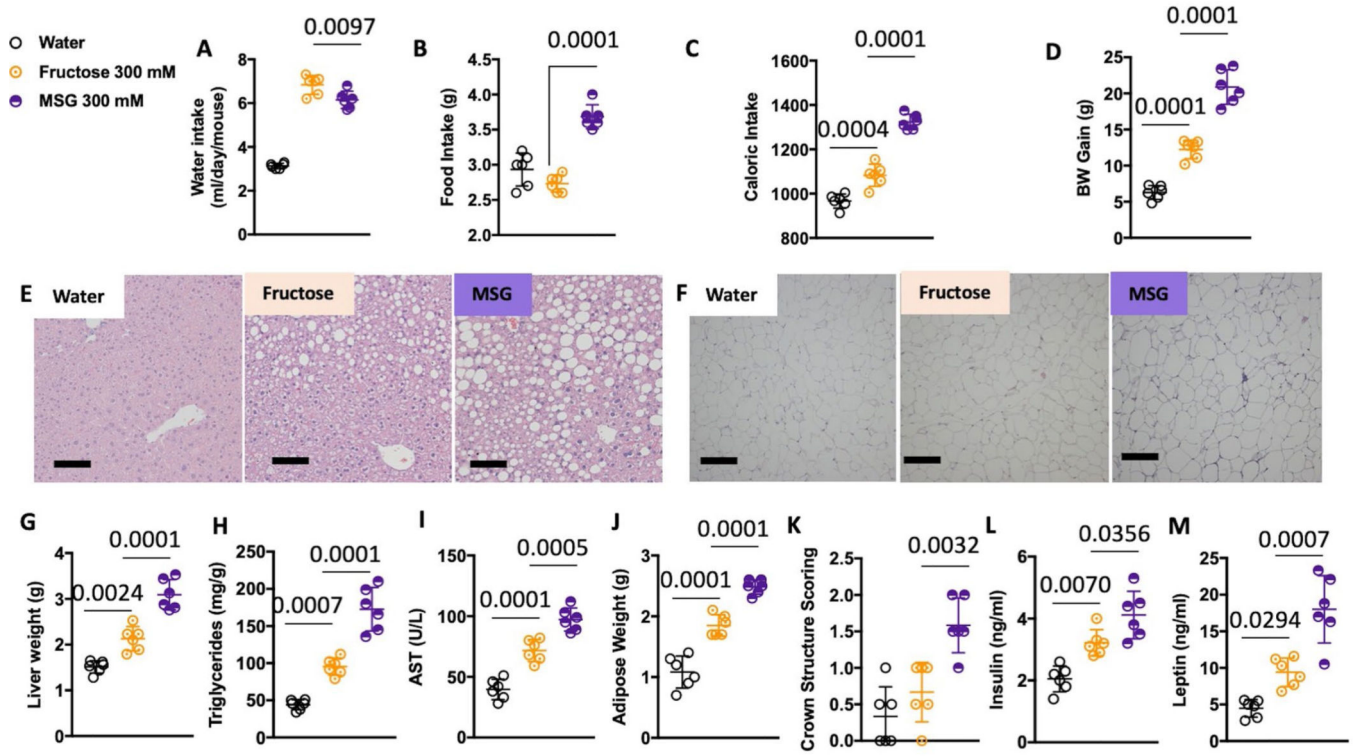

Extended Data Fig. 1 |. MSG is a more potent inducer of metabolic syndrome than fructose. **A)** Mean daily water intake, **B)** daily food intake and **C)** total caloric intake in wild type mice on water control or exposed to the same amount of fructose or MSG (300 mM) for 15 weeks. **D)** Body weight gain in the same groups as in A). **E)** Representative H&E images of liver and **F)** epididymal adipose in the same groups as in A). Size bar: 20 μm **G)** Liver weight, **H)** intrahepatic triglycerides and **I)** plasma AST levels in the same groups as in A). **J)** Epididymal adipose weight and **K)** crown structure scoring as well as **L)** fasting plasma levels of insulin and **M)** leptin in the same groups as in A). Data in A-B and D-M represent

individual points with mean ± SEM. Data in C represent mean ± SEM. One Way ANOVA. N = 6 mice per group.

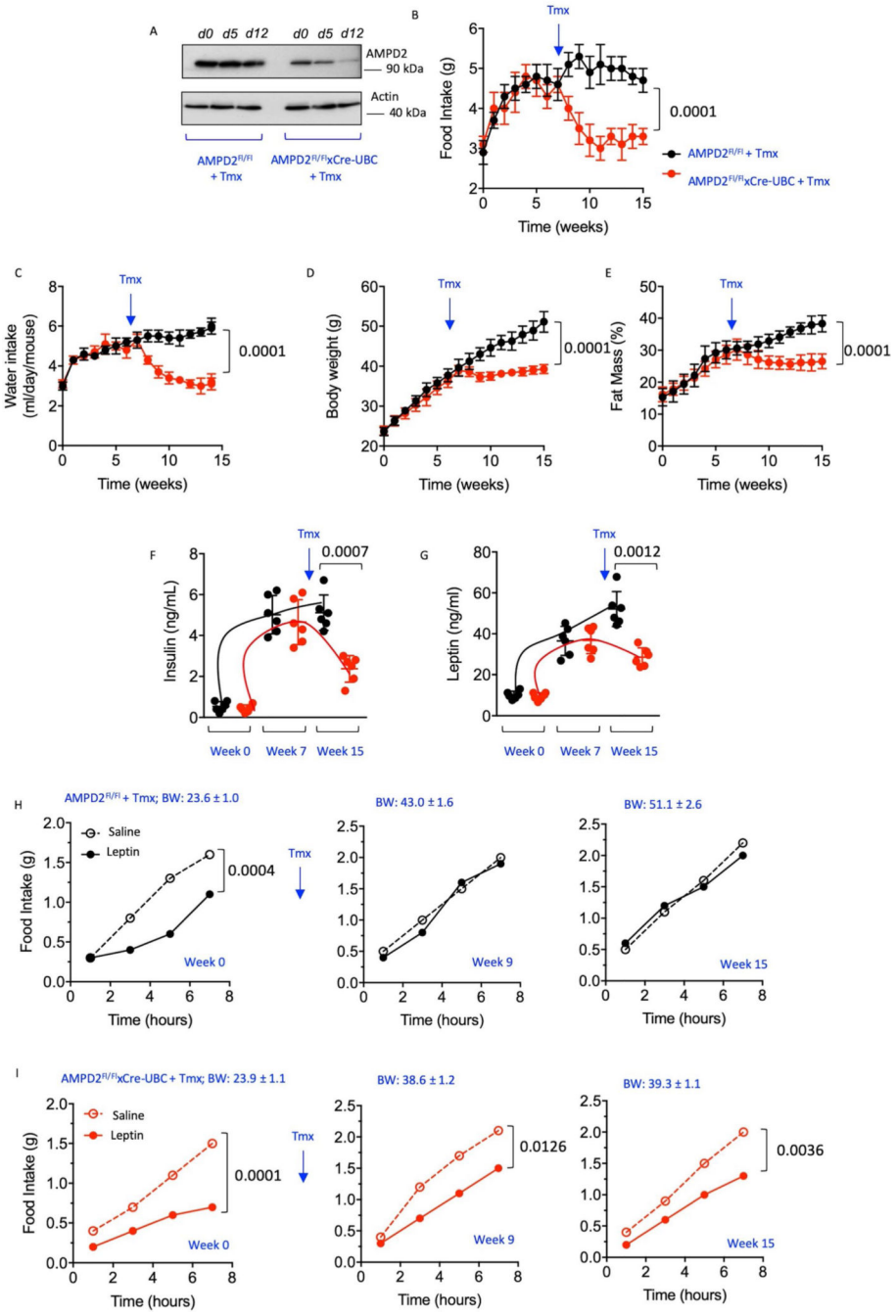

Extended Data Fig. 2 |. Tamoxifen does not interfere in metabolic syndrome induced by MSG. **A)** Representative western blot in liver for AMPD2 (top) and actin loading control (bottom) in tamoxifen-resistant AMPD2$^{Fl/FL}$ mice and tamoxifen-inducible AMPD2 knockout mice (AMPD2$^{Fl/FL}$xCre-UBC) at days 0, 5 and 12 after tamoxifen treatment. **B)** Seven hour food intake in AMPD2$^{Fl/FL}$ (black) and AMPD2$^{Fl/FL}$xCre-UBC (red) mice before (weeks

0 to week 7) and after (week 7 to week 15) tamoxifen (TMX) treatment **C)** MSG solution drinking in the same groups as in B) **D)** Body weight gain in in the same groups as in B) **E)** Fat/fat free mass ratio in in the same groups as in B) **F)** Fasting plasma insulin in AMPD2$^{Fl/FL}$ (black) and AMPD2$^{Fl/FL}$xCre-UBC (red) mice at baseline (week 0), before TMX treatment (week 7) and after TMX treatment (week 15). **G)** Fasting plasma leptin levels in the same groups as in G). **H)** Leptin sensitivity in AMPD2$^{Fl/FL}$ mice at baseline (week 0), and after TMX treatment (weeks 9 and 15). **I)** Leptin sensitivity in AMPD2$^{Fl/FL}$xCre-UBC mice at baseline (week 0), before TMX treatment (weeks 9 and 15). Data in F-G represent individual points with mean ± SEM. Data in B-E represent mean ± SEM. Data in H-I represent the mean. One Way ANOVA (F-G) and 2-tail t-test (A-E and H-I). N = 6 mice per group.

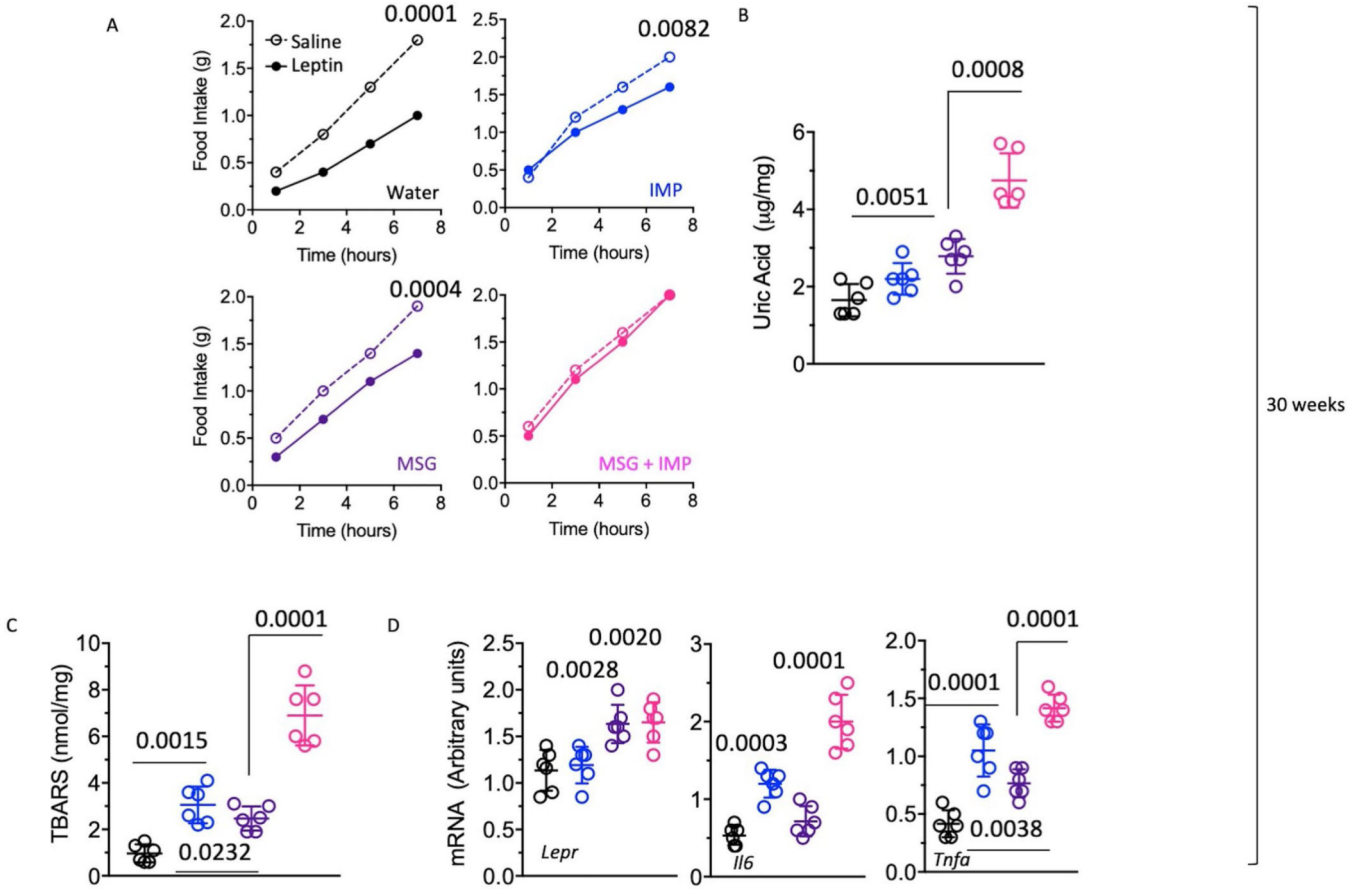

Extended Data Fig. 3 |. Leptin sensitivity in wild type mice exposed to MSG + IMP for 30 weeks. **A)** Seven hour food intake after leptin injection in mice on water control, or exposed to IMP (300 µM), MSG (30 mM) or a MSG + IMP combination for 30 weeks and injected with leptin. **B)** Hypothalamic uric acid and **C)** TBAR levels in mice on water control, or exposed to IMP (300 µM), MSG (30 mM) or a MSG + IMP combination for 15 weeks. **D)** Hypothalamic mRNA levels of the leptin receptor (*lepr*), and cytokines *il6* and *tnfa*. Data in B-D represent individual points with mean ± SEM. Data in A represent the meanOne Way ANOVA (B-D) and 2-tail t-test (A). N = 6 mice per group.

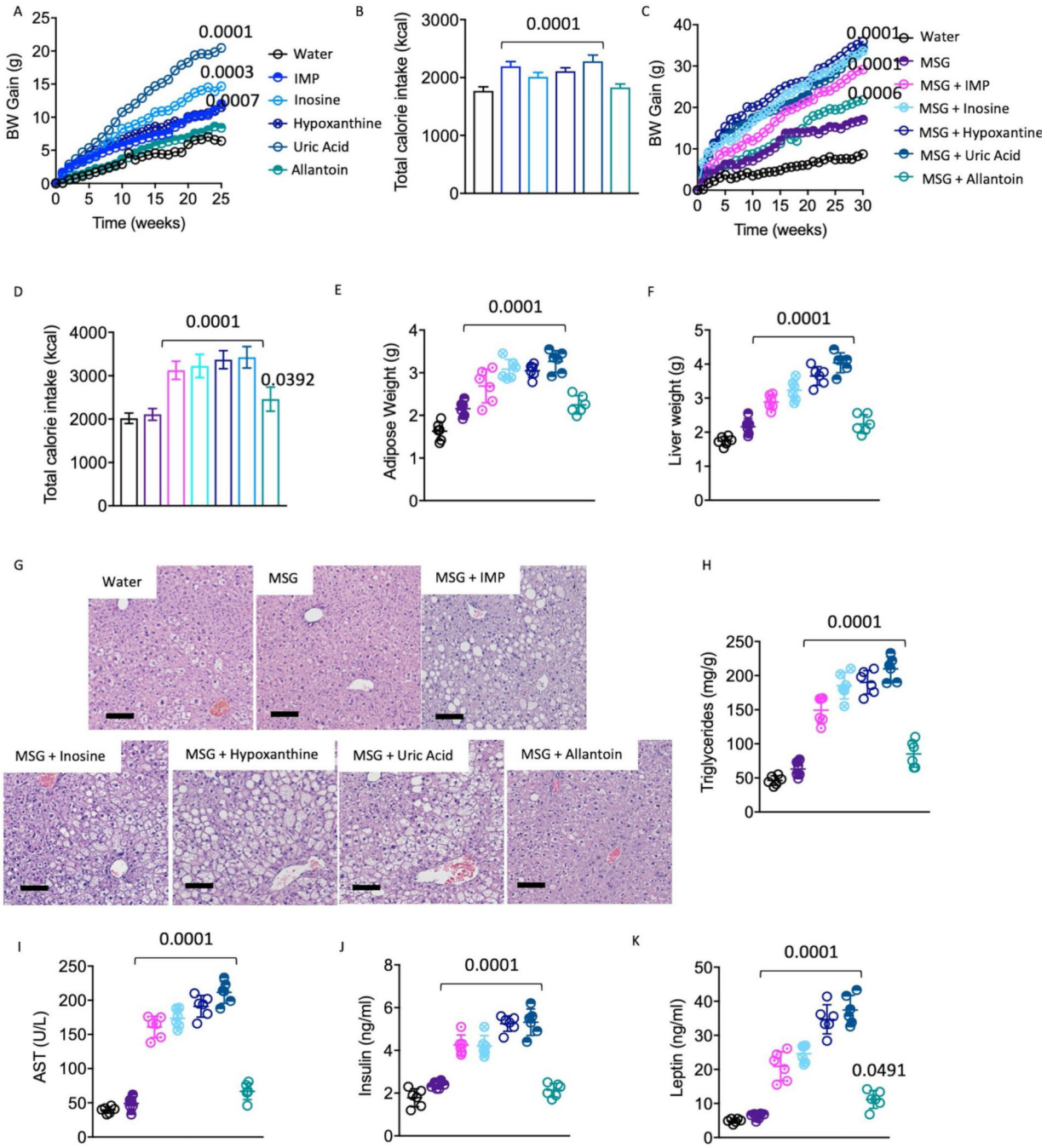

Extended Data Fig. 4 |. Downstream products of IMP exacerbate MSG-induced metabolic syndrome.

A) Body weight gain and **B)** cumulative total caloric intake in wild type mice on water control, or exposed to IMP, inosine, hypoxanthine, uric acid or allantoin (300 μM) for 30 weeks. **C)** Body weight gain and **D)** total caloric intake in wild type mice on water control, or exposed to MSG (30 mM) alone or in combination with IMP, inosine, hypoxanthine, uric acid or allantoin (300 μM) for 30 weeks. **E)** Epididymal adipose weight, **F)** liver weight, **G)** representative H&E images of liver, **H)** intrahepatic triglycerides and **I)** plasma AST, **J)**

insulin and **K)** leptin levels in wild type mice of the same groups as in C). Size bar: 20 μm. Data in E-F, H-K represent individual points with mean ± SEM. Data in B and D represent mean ± SEM. Data in A and C represent the meanOne Way ANOVA. N = 6 mice per group.

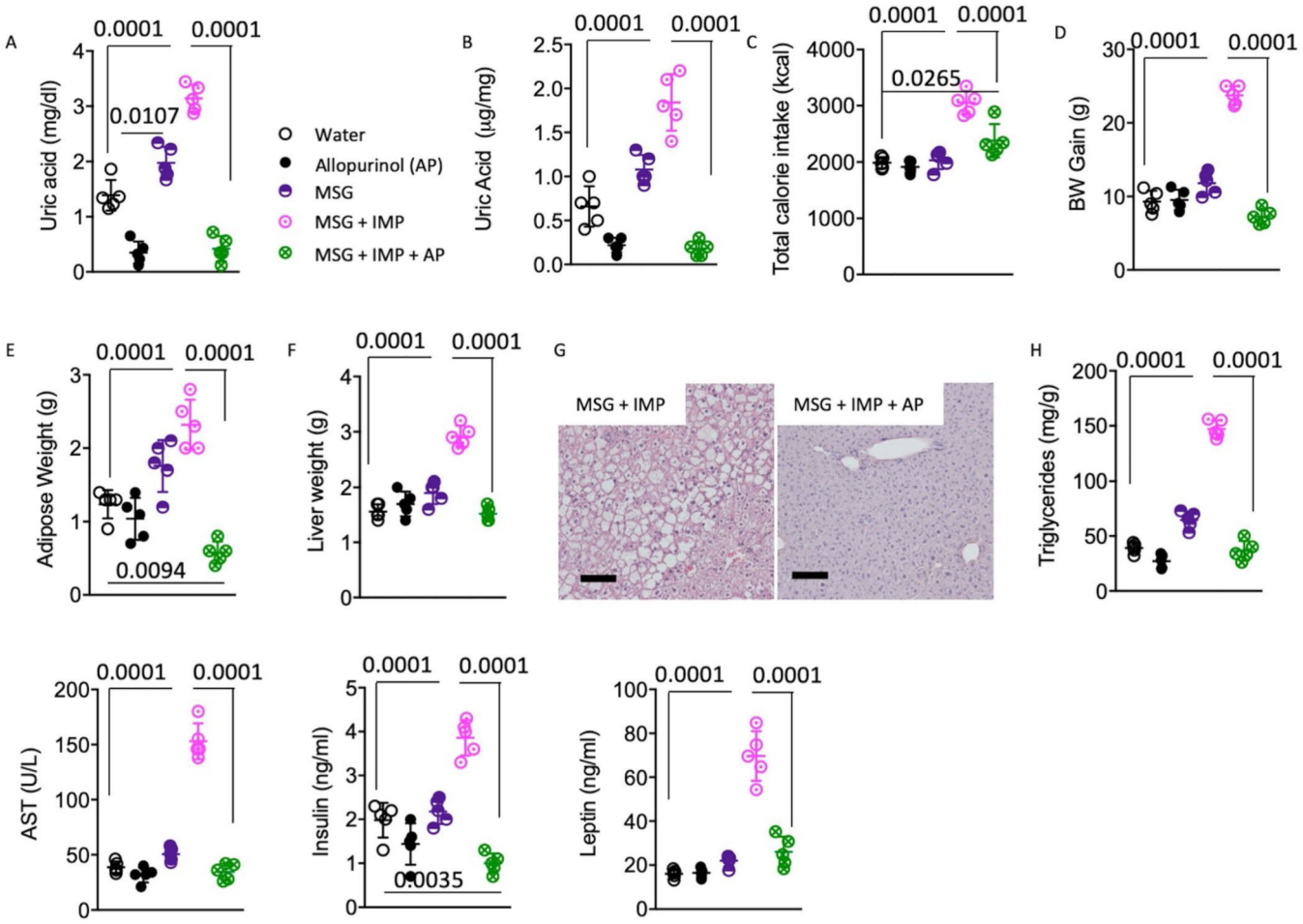

Extended Data Fig. 5 |. Allopurinol ameliorates metabolic syndrome induced by MSG + IMP. **A)** Plasma and **B)** intrahepatic uric acid levels in wild type mice on water control, allopurinol (AP, 1.1 mM), MSG (30 mM) alone, or in combination with IMP (300 μM) or IMP + allopurinol (AP, 1.1 mM) for 30 weeks. **C)** Cumulative total caloric intake and **D)** body weight gain in the same mice as in A). **E)** Epididymal adipose weight, **F)** liver weight, **G)** representative H&E images of liver, **H)** intrahepatic triglycerides and **I)** plasma AST, **J)** insulin and **K)** leptin levels in wild type mice of the same groups as in A). Size bar: 20 μm. Data in A-B and D-K represent individual points with mean ± SEM. Data in C represent mean ± SEMOne Way ANOVA (A-C, F, H-J and N-O) and 2-tail t-test (D-E, G, K-M and P-Q). N = 6 mice per group.

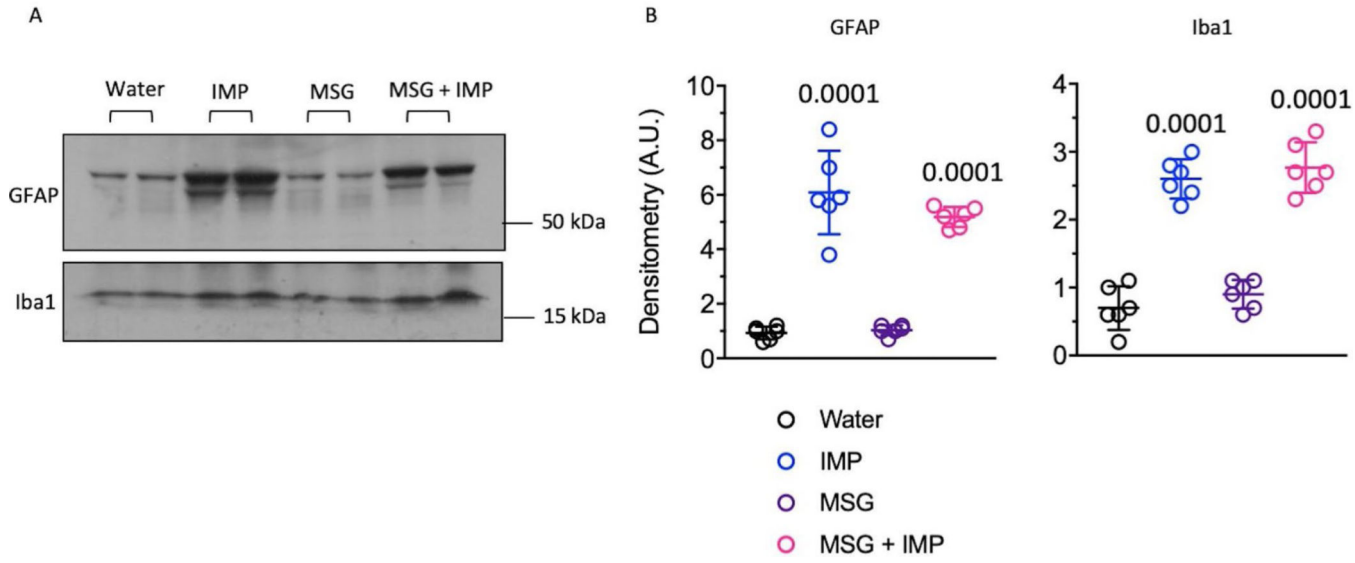

Extended Data Fig. 6 |. MSG and IMP activate astrocytes and microglia in the hypothalamus.
A) Representative western blot and **B)** densitometry for GFAP (astrocyte marker), Iba1 (microglia marker) and actin loading control in hypothalamus of wild type mice exposed to water, IMP, MSG (30 mM) or MSG + IMP. Data in B-C represent individual points with mean ± SEM. One Way ANOVA. N = 6 mice per group.

Supplementary Material

Refer to Web version on PubMed Central for supplementary material.

Acknowledgements

We thank E. E. Smith for her contribution to this research and A. Quador and J. Arnold of the University of Colorado Denver Histology Shared Resource. This resource is supported in part by the Cancer Center Support Grant (no. P30CA046934). This work has been supported by NIH grant nos. 1R01DK121496-01A1 (to M.A.L. and R.J.J.) and 1R01DK108859 (to M.A.L.). A.A.H was supported by funding from the Colorado Nutrition Obesity Research Center (no. 25M9260) from parental grant P30DK048520.

References

1. Beauchamp GK & Mennella JA Flavor perception in human infants: development and functional significance. Digestion 83, 1–6 (2011).
2. Stanhope KL et al. Consumption of fructose and high fructose corn syrup increase postprandial triglycerides, LDL-cholesterol, and apolipoprotein-B in young men and women. J. Clin. Endocrinol. Metab 96, E1596–E1605 (2011). [PubMed: 21849529]
3. Stanhope KL et al. Consuming fructose-sweetened, not glucose-sweetened, beverages increases visceral adiposity and lipids and decreases insulin sensitivity in overweight/obese humans. J. Clin. Invest 119, 1322–1334 (2009). [PubMed: 19381015]
4. Ishimoto T. et al. Opposing effects of fructokinase C and A isoforms on fructose-induced metabolic syndrome in mice. Proc. Natl Acad. Sci. USA 109, 4320–4325 (2012). [PubMed: 22371574]
5. Schwarz J-M et al. Effects of dietary fructose restriction on liver fat, de novo lipogenesis, and insulin kinetics in children with obesity. Gastroenterology 153, 743–752 (2017). [PubMed: 28579536]

6. Johnson RJ et al. Fructose metabolism as a common evolutionary pathway of survival associated with climate change, food shortage and droughts. J. Intern. Med 287, 252–262 (2020). [PubMed: 31621967]
7. Yang Q. et al. Added sugar intake and cardiovascular diseases mortality among US adults. JAMA Intern. Med 174, 516–524 (2014). [PubMed: 24493081]
8. Hulthén L. et al. Salt intake in young Swedish men. Public Health Nutr. 13, 601–605 (2010). [PubMed: 19968896]
9. Libuda L, Kersting M. & Alexy U. Consumption of dietary salt measured by urinary sodium excretion and its association with body weight status in healthy children and adolescents. Public Health Nutr. 15, 433–441 (2012). [PubMed: 21929845]
10. Choi Y. et al. Dietary sodium and potassium intake in relation to non-alcoholic fatty liver disease. Br. J. Nutr 116, 1447–1456 (2016). [PubMed: 27725000]
11. Lanaspa MA et al. High salt intake causes leptin resistance and obesity in mice by stimulating endogenous fructose production and metabolism. Proc. Natl Acad. Sci. USA 115, 3138–3143 (2018). [PubMed: 29507217]
12. Lanaspa MA et al. Counteracting roles of AMP deaminase and AMP kinase in the development of fatty liver. PLoS ONE 7, e48801 (2012).
13. Lanaspa MA et al. Uric acid induces hepatic steatosis by generation of mitochondrial oxidative stress: potential role in fructose-dependent and -independent fatty liver. J. Biol. Chem 287, 40732–40744 (2012). [PubMed: 23035112]
14. Cicerchi C. et al. Uric acid-dependent inhibition of AMP kinase induces hepatic glucose production in diabetes and starvation: evolutionary implications of the uricase loss in hominids. FASEB J. 28, 3339–3350 (2014). [PubMed: 24755741]
15. Feigelson M. & Feigelson P. Relationships between hepatic enzyme induction, glutamate formation, and purine nucleotide biosynthesis in glucocorticoid action. J. Biol. Chem 241, 5819–5826 (1966). [PubMed: 4380931]
16. Zhang F. et al. Molecular mechanism for the umami taste synergism. Proc. Natl Acad. Sci. USA 105, 20930–20934 (2008). [PubMed: 19104071]
17. Johnson RJ et al. Umami: the taste that drives purine intake. J. Rheumatol 40, 1794–1796 (2013). [PubMed: 24187156]
18. Minami S, Sato M, Shiraiwa Y. & Iwamoto K. Molecular characterization of adenosine 5′-monophosphate deaminase—the key enzyme responsible for the umami taste of nori (Porphyra yezoensis Ueda, Rhodophyta). Mar. Biotechnol. (NY) 13, 1140–1147 (2011). [PubMed: 21519809]
19. He K. et al. Consumption of monosodium glutamate in relation to incidence of overweight in Chinese adults: China Health and Nutrition Survey (CHNS). Am. J. Clin. Nutr 93, 1328–1336 (2011). [PubMed: 21471280]
20. Insawang T. et al. Monosodium glutamate (MSG) intake is associated with the prevalence of metabolic syndrome in a rural Thai population. Nutr. Metab. (Lond.) 9, 50 (2012). [PubMed: 22681873]
21. Bunyan J, Murrell EA & Shah PP The induction of obesity in rodents by means of monosodium glutamate. Br. J. Nutr 35, 25–39 (1976). [PubMed: 1106764]
22. Collison KS et al. Effect of dietary monosodium glutamate on HFCS-induced hepatic steatosis: expression profiles in the liver and visceral fat. Obesity (Silver Spring) 18, 1122–1134 (2010). [PubMed: 20111022]
23. López-Miranda V. et al. Effects of chronic dietary exposure to monosodium glutamate on feeding behavior, adiposity, gastrointestinal motility, and cardiovascular function in healthy adult rats. Neurogastroenterol. Motil 27, 1559–1570 (2015). [PubMed: 26303145]
24. Nakamura H, Kawamata Y, Kuwahara T, Smriga M. & Sakai R. Long-term ingestion of monosodium L-glutamate did not induce obesity, dyslipidemia or insulin resistance: a two-generation study in mice. J. Nutr. Sci. Vitaminol. (Tokyo) 59, 129–135 (2013). [PubMed: 23727643]

25. Andres-Hernando A. et al. Deletion of fructokinase in the liver or in the intestine reveals differential effects on sugar-induced metabolic dysfunction. Cell Metab. 32, 117–127.e3 (2020). [PubMed: 32502381]
26. Murata Y, Beauchamp GK & Bachmanov AA Taste perception of monosodium glutamate and inosine monophosphate by 129P3/J and C57BL/6ByJ mice. Physiol. Behav 98, 481–488 (2009). [PubMed: 19666040]
27. Schiffman SS, Sattely-Miller EA, Zimmerman IA, Graham BG & Erickson RP Taste perception of monosodium glutamate (MSG) in foods in young and elderly subjects. Physiol. Behav 56, 265–275 (1994). [PubMed: 7938237]
28. Shapiro A. et al. Fructose-induced leptin resistance exacerbates weight gain in response to subsequent high-fat feeding. Am. J. Physiol. Regul. Integr. Comp. Physiol 295, R1370–R1375 (2008). [PubMed: 18703413]
29. Sautin YY, Nakagawa T, Zharikov S. & Johnson RJ Adverse effects of the classic antioxidant uric acid in adipocytes: NADPH oxidase-mediated oxidative/nitrosative stress. Am. J. Physiol. Cell Physiol 293, C584–C596 (2007). [PubMed: 17428837]
30. Johnson RJ et al. Fructose metabolism as a common evolutionary pathway of survival associated with climate change, food shortage and droughts. J. Intern. Med 287, 252–262 (2020). [PubMed: 31621967]
31. Hudoyo AW et al. Role of AMPD2 in impaired glucose tolerance induced by high fructose diet. Mol. Genet. Metab. Rep 13, 23–29 (2017). [PubMed: 28765812]
32. Clifford AJ, Riumallo JA, Youn VR & Scrimshaw NS Effect of oral purines on serum and urinary uric acid of normal, hyperuricemic and gouty humans. J. Nutr 106, 428–434 (1976).
33. Lu W. et al. Uric acid produces an inflammatory response through activation of NF-κB in the hypothalamus: implications for the pathogenesis of metabolic disorders. Sci. Rep 5, 12144 (2015). [PubMed: 26179594]
34. Sanchez-Lozada LG et al. Uric acid activates aldose reductase and the polyol pathway for endogenous fructose and fat production causing development of fatty liver in rats. J. Biol. Chem 294, 4272–4281 (2019). [PubMed: 30651350]
35. Lanaspa MA et al. Uric acid stimulates fructokinase and accelerates fructose metabolism in the development of fatty liver. PLoS ONE 7, e47948 (2012).
36. National Research Council of the National Academies. Guide for the Care and Use of Laboratory Animals (National Academies Press, 2011).
37. Lanaspa MA et al. Opposing activity changes in AMP deaminase and AMP-activated protein kinase in the hibernating ground squirrel. PLoS ONE 10, e0123509 (2015).
38. Lanaspa MA et al. The tight junction protein, MUPP1, is up-regulated by hypertonicity and is important in the osmotic stress response in kidney cells. Proc. Natl Acad. Sci. USA 104, 13672–13677 (2007). [PubMed: 17690246]

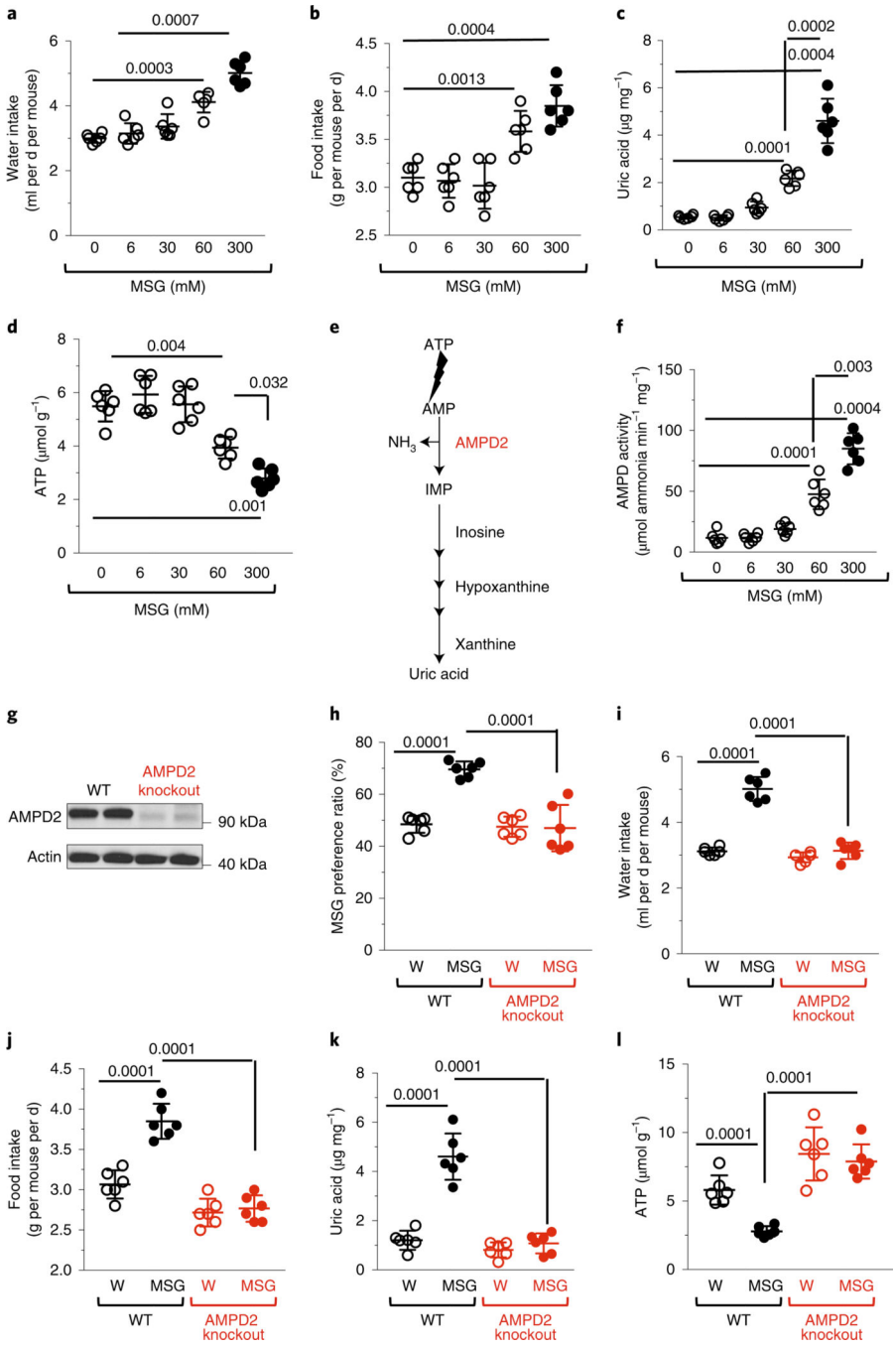

Fig. 1 |. MSG stimulates intake by promoting nucleotide turnover and purine degradation into uric acid.

a–d, Mean water intake (**a**), mean daily food intake (two weeks) (**b**), intrahepatic uric acid levels (**c**) and intrahepatic ATP acid levels (**d**) in mice exposed to increased concentrations of MSG. **e**, Schematic depicting the purine degradation pathway from AMP. AMP produced from the degradation of ATP is deaminized to IMP by AMPD2. IMP is then degraded to uric acid through several enzymatic reactions, producing intermediate products including inosine, hypoxanthine and xanthine. **f**, Intrahepatic AMPD activity in mice exposed to

increased concentrations of MSG. **g**, Representative western blot against AMPD2 and actin control from liver extracts from WT and AMPD2 knockout mice. **h**, Water/MSG (300 mM) preference ratios in WT and AMPD2 knockout mice. **i**–**l**, Daily water intake (**i**), daily food intake (**j**), intrahepatic uric acid levels (**k**) and intrahepatic ATP levels (**l**) in WT and AMPD2 knockout mice exposed 300 mM of MSG. Data represent individual points with the mean ± s.e.m. One-way ANOVA analysis. $n = 6$ mice per group.

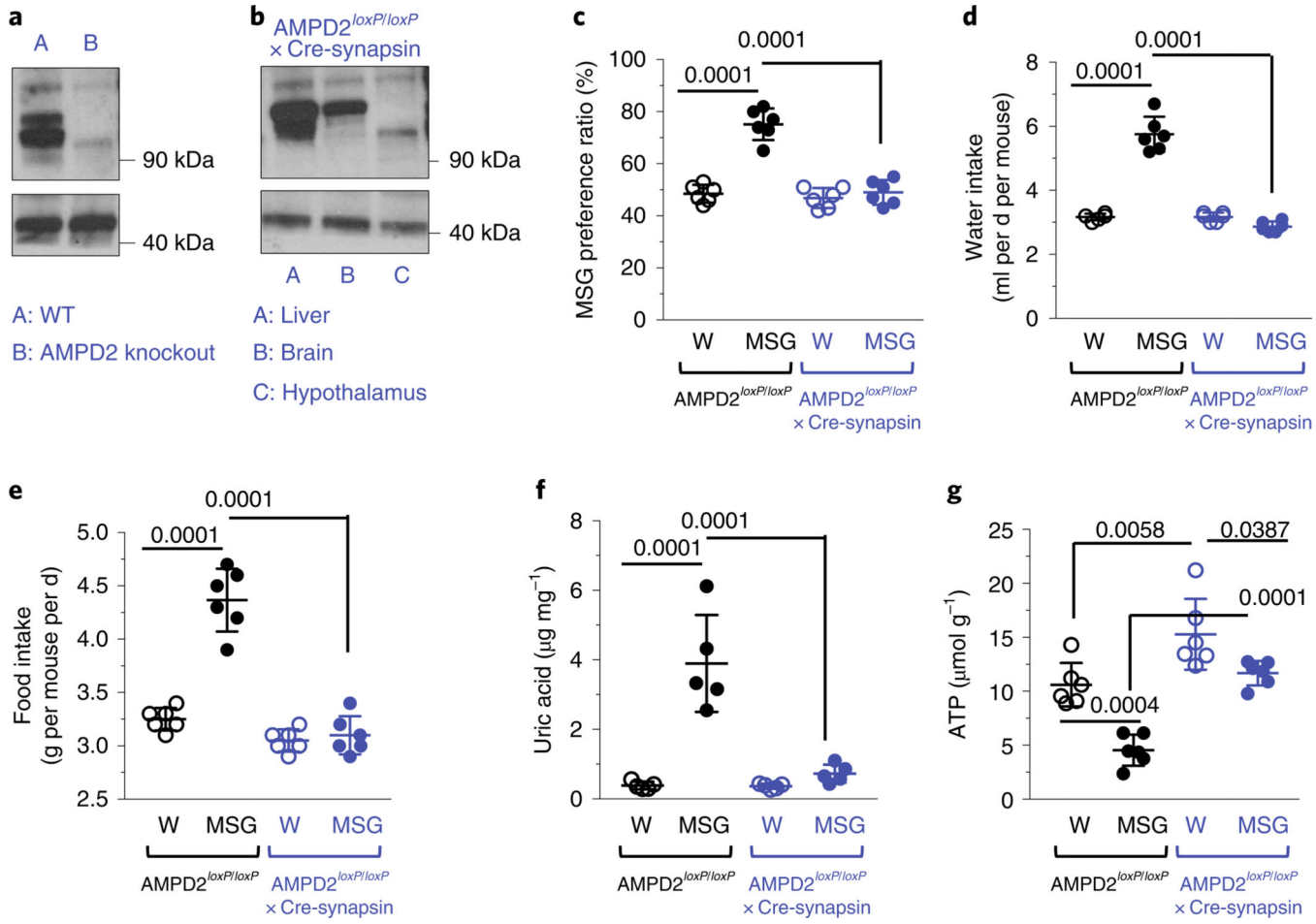

Fig. 2 |. Neuronal AMPD2 drives the intake of MSG and total calories.

a, Representative western blot for AMPD2 (top) and actin loading control (bottom) in WT and whole-body AMPD2 knockout mice. **b**, Representative western blot for AMPD2 (top) and actin loading control (bottom) in neuron-specific AMPD2 knockout mice (AMPD2$^{loxP/loxP}$ × Cre-synapsin) in liver (not silenced), whole brain and hypothalamus. Neuron-specific AMPD2 knockout mice demonstrated a much greater depletion in AMPD2 expression in hypothalamic areas compared to whole brain. **c**, MSG/water preference ratio in AMPD2$^{loxP/loxP}$ control mice and neuron-specific AMPD2 knockout mice (MSG 300 mM). **d**, MSG solution drinking in AMPD2$^{loxP/loxP}$ control mice and neuron-specific AMPD2 knockout mice. **e**, Mean daily food intake in control and MSG-receiving AMPD2$^{loxP/loxP}$ control mice and neuron-specific AMPD2 knockout mice. **f**, Hypothalamic uric acid levels in control and MSG-receiving AMPD2$^{loxP/loxP}$ control mice and neuron-specific AMPD2 knockout mice. **g**, Hypothalamic ATP levels in control and MSG-receiving AMPD2$^{loxP/loxP}$ control mice and neuron-specific AMPD2 knockout mice. Data represent individual points with the mean ± s.e.m. One-way ANOVA. $n = 6$ mice per group.

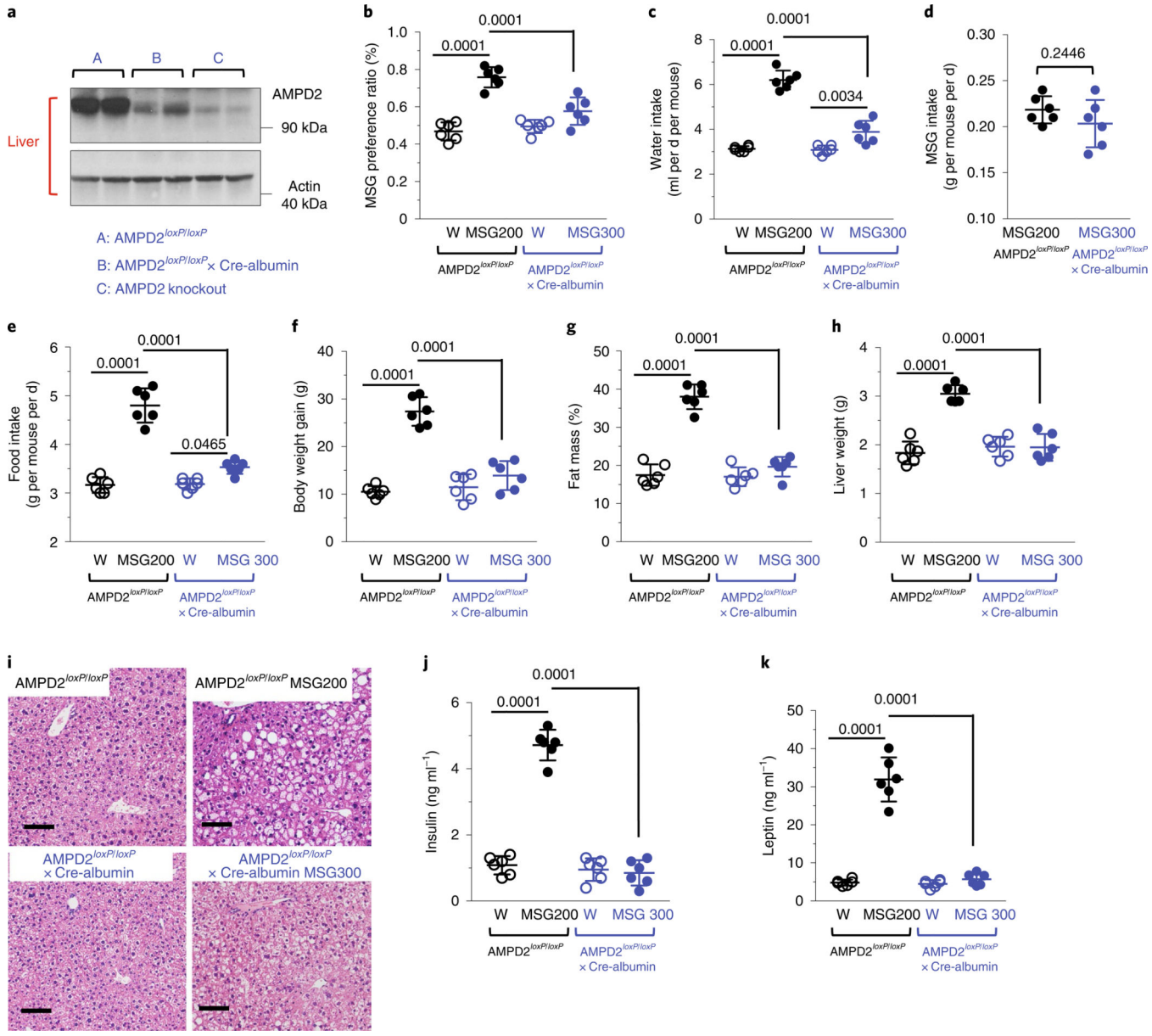

Fig. 3 |. Hepatocyte-specific AMPD2 drives MSG-induced metabolic syndrome and intake.

a, Representative western blot in liver and control kidney lysates for AMPD2 (top) and actin loading control (bottom) in control AMPD2$^{loxP/loxP}$, liver-specific AMPD2 knockout mice (AMPD2$^{loxP/loxP}$ × Cre-albumin) and whole-body AMPD2 knockout mice. **b**, MSG/water preference ratio in AMPD2$^{loxP/loxP}$ control mice and liver-specific AMPD2 knockout mice. **c**–**e**, MSG solution drinking in AMPD2$^{loxP/loxP}$ control (200 mM) mice and liver-specific AMPD2 knockout mice (300 mM) (**c**), daily MSG consumption in matched AMPD2$^{loxP/loxP}$ control (200 mM) mice and liver-specific AMPD2 knockout mice (**d**) and mean daily food intake (**e**) in control and MSG-receiving AMPD2$^{loxP/loxP}$ mice and liver-specific AMPD2 knockout mice. **f**–**h**, Body weight gain (**f**), fat/fat-free mass ratio (**g**) and liver weight (**h**) in control and MSG-receiving AMPD2$^{loxP/loxP}$ control mice and liver-specific AMPD2 knockout mice. **i**, Representative H&E liver images in control and MSG-receiving

AMPD2$^{loxP/loxP}$ mice and liver-specific AMPD2 knockout mice. Size bar, 20 μm. **j**,**k**, Plasma insulin (**j**) and leptin (**k**) levels in control and MSG-receiving AMPD2$^{loxP/loxP}$ mice and liver-specific AMPD2 knockout mice. Data represent individual points with the mean ± s.e.m. One-way ANOVA. n = 6 mice per group.

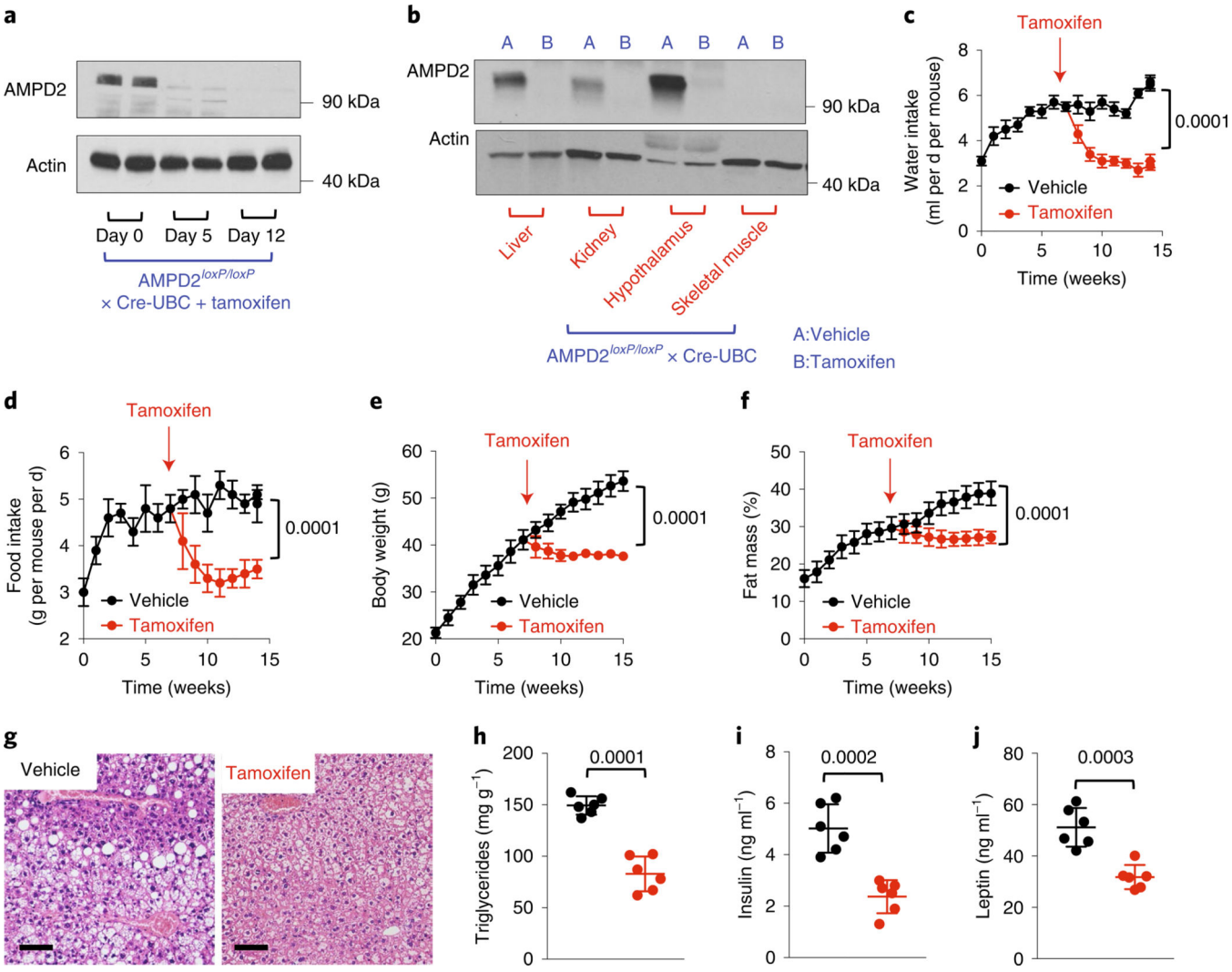

Fig. 4 |. AMPD2 deletion ameliorates metabolic syndrome in MSG-receiving adult mice.

a, Representative western blot in the liver for AMPD2 (top) and actin (bottom) loading control in tamoxifen-inducible AMPD2 knockout mice (AMPD2$^{loxP/loxP}$ × Cre-UBC) at days 0, 5 and 12 after tamoxifen treatment. **b**, Representative western blot in the liver, kidney hypothalamus and skeletal muscle (negative control for AMDP2 expression) for AMPD2 (top) and actin (bottom) loading control in tamoxifen-inducible AMPD2 knockout mice (AMPD2$^{loxP/loxP}$ × Cre-UBC) at day 12 after receiving vehicle (A) or tamoxifen (B) treatment. **c**, MSG solution drinking in AMPD2$^{loxP/loxP}$ × Cre-UBC mice after vehicle (black) or tamoxifen (red) treatment. **d**, Daily food intake in AMPD2$^{loxP/loxP}$ × Cre-UBC mice after vehicle (black) or tamoxifen (red) treatment. **e**, Body weight gain in AMPD2$^{loxP/loxP}$ × Cre-UBC mice after vehicle (black) or tamoxifen (red) treatment. **f**, Fat/fat-free mass ratio in AMPD2$^{loxP/loxP}$ × Cre-UBC mice after vehicle (black) or tamoxifen (red) treatment. **g**, Representative H&E liver images in AMPD2$^{loxP/loxP}$ × Cre-UBC mice after vehicle (black) or tamoxifen (red) treatment. Size bar, 20 μm. **h**–**j**, Liver triglycerides (**h**), plasma insulin (**i**) and leptin (**j**) levels in AMPD2$^{loxP/loxP}$ × Cre-UBC mice after vehicle (black) or tamoxifen (red) treatment. **h**–**j**, Data represent individual points with the mean

± s.e.m. **c**–**f**, Data represent the mean ± s.e.m. One-way ANOVA (**h**–**j**) or two-tailed *t*-test (**c**–**f**). $n = 6$ mice per group.

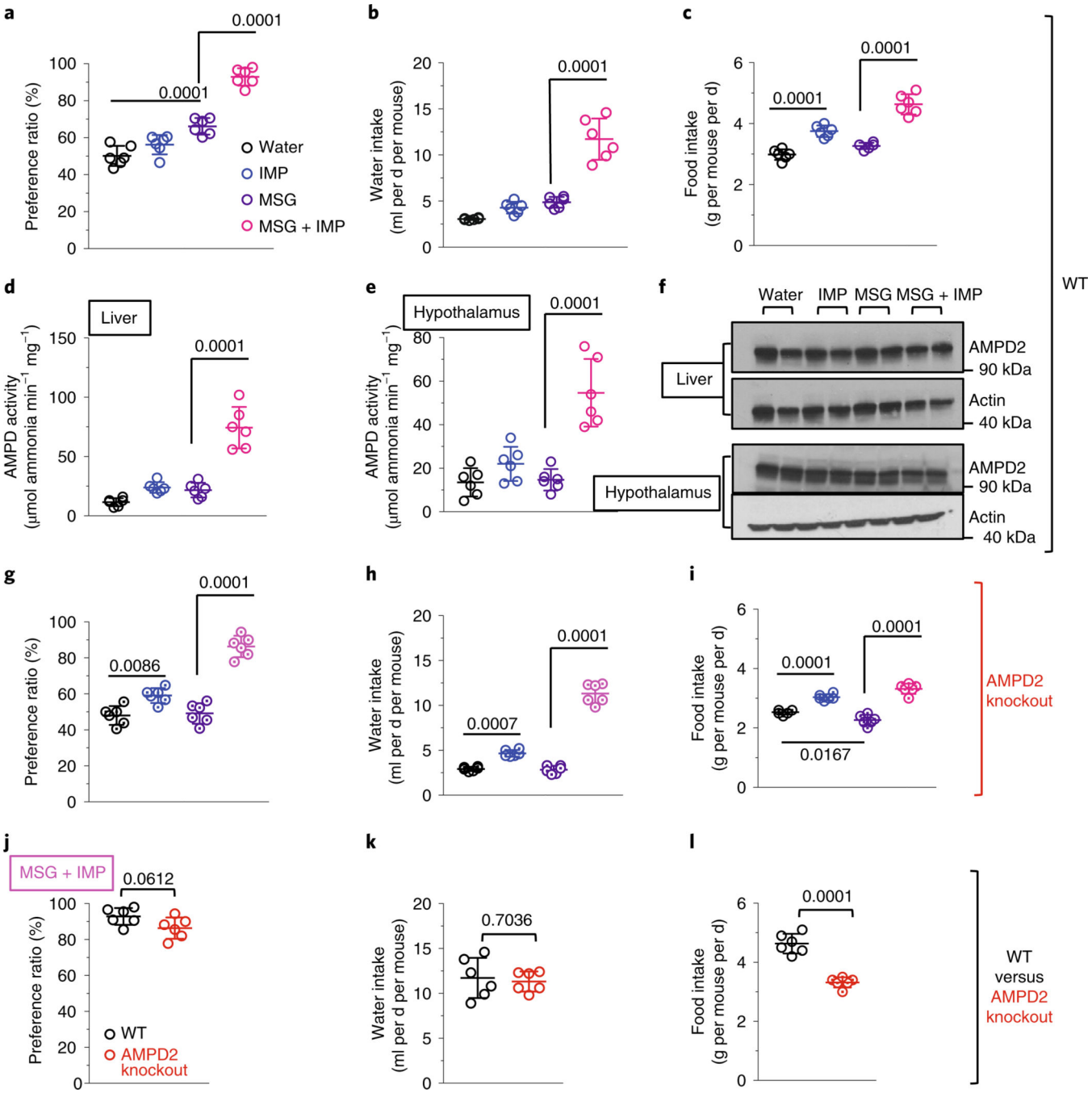

Fig. 5 |. IMP exacerbates MSG-mediated preference and food intake in WT and AMPD2 knockout mice.

a–c, Preference ratio (**a**), mean daily water intake (**b**) and mean daily food intake (**c**) in WT mice on water control or exposed to IMP (300 μM), MSG (30 mM) or an MSG + IMP combination. **d**,**e**, AMPD activity in the liver (**d**) and hypothalamus (**e**) of mice exposed to IMP (300 μM), MSG (30 mM) or an MSG + IMP combination. **f**, Representative western blot for AMPD2 and actin loading control in the liver and hypothalamus of mice exposed to IMP (300 μM), MSG (30 mM) or an MSG + IMP combination. **g–i**, Preference ratio (**g**),

mean daily water intake (**h**) and mean daily food intake (**i**) in AMPD2 knockout mice on water control or exposed to IMP (300 μM), MSG (30 mM) or an MSG + IMP combination. **j**–**l**, Preference ratio (**j**), daily water intake (**k**) and daily food intake (**l**) in WT and AMPD2 knockout mice exposed to an MSG + IMP combination. For these studies, a two-bottle preference test was used for the studies reported in Fig. 5a,d,g. The remaining studies were done using a single-bottle preference test. Data represent individual points with the mean ± s.e.m. One-way ANOVA. $n = 6$ mice per group.

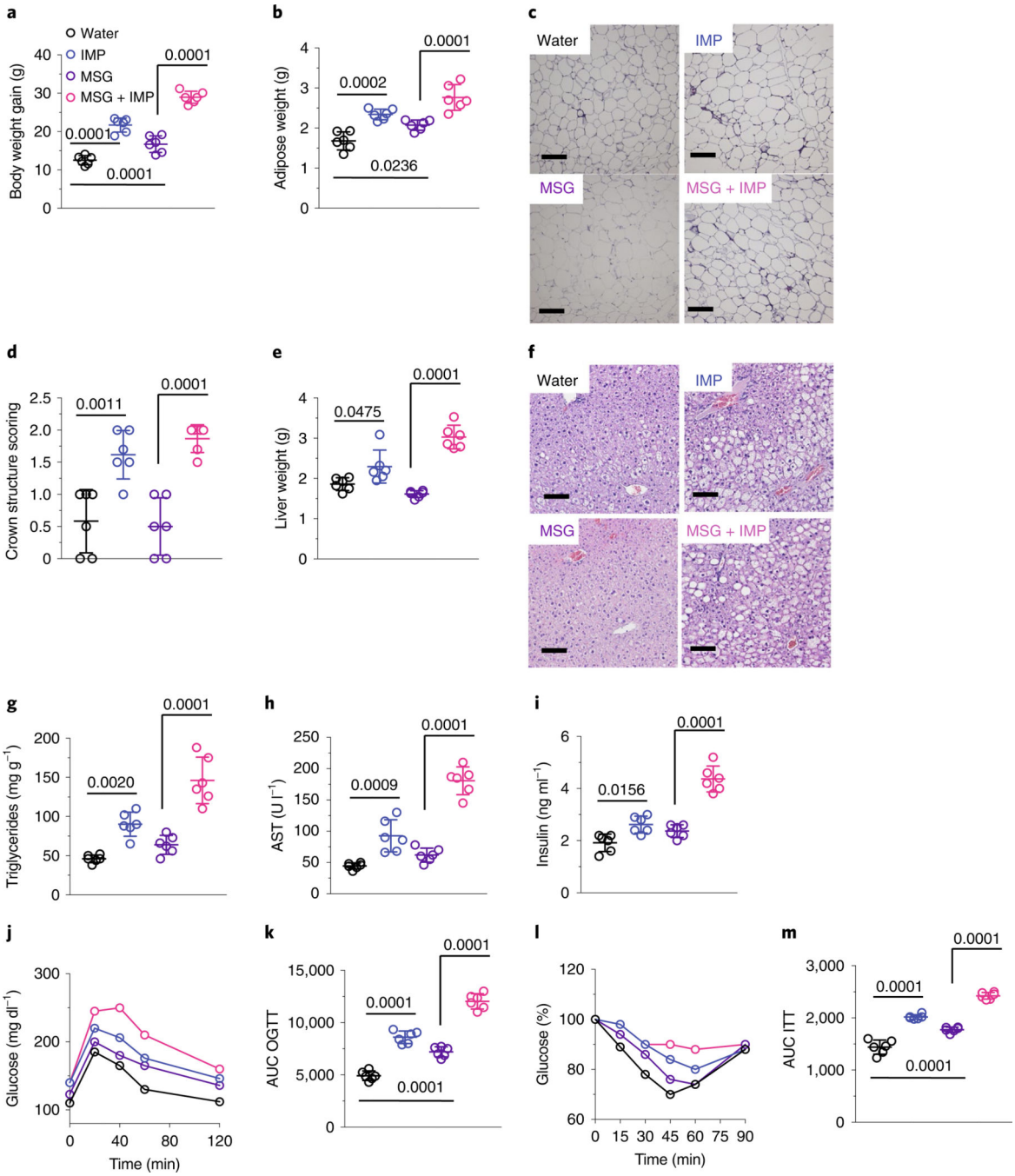

Fig. 6 |. MSG + IMP combination induces metabolic syndrome in mice.

a, Body weight gain of WT mice on water control or if exposed to IMP (300 μM), MSG (30 mM) or an MSG + IMP combination for 30 weeks. **b**–**d**, Epididymal adipose weight (**b**), representative H&E images of epididymal adipose weight (**c**) and adipose crown structure scoring (**d**) in WT mice of the same groups as in **a**. Size bar, 20 μm. **e**–**i**, Liver weight (**e**), representative H&E images of liver (**f**), intrahepatic triglycerides (**g**), plasma AST levels (**h**) and fasting insulin (**i**) in WT mice of the same groups as in **a**. Size bar, 20 μm. **j**,**k**, Plasma glucose (**j**) and area under the curve (AUC) (**k**) in WT mice of the same groups as in **a** under

OGTTs. **l**,**m**, Plasma glucose (**l**) and AUC (**m**) in WT mice of the same groups as in **a** under ITTs. **a**–**k**,**l**,**m**, Data represent individual points with the mean ± s.e.m. **j**,**l**, Data represent the mean ± s.e.m. **a**–**k**,**i**,**m**, One-way ANOVA. n = 6 mice per group.

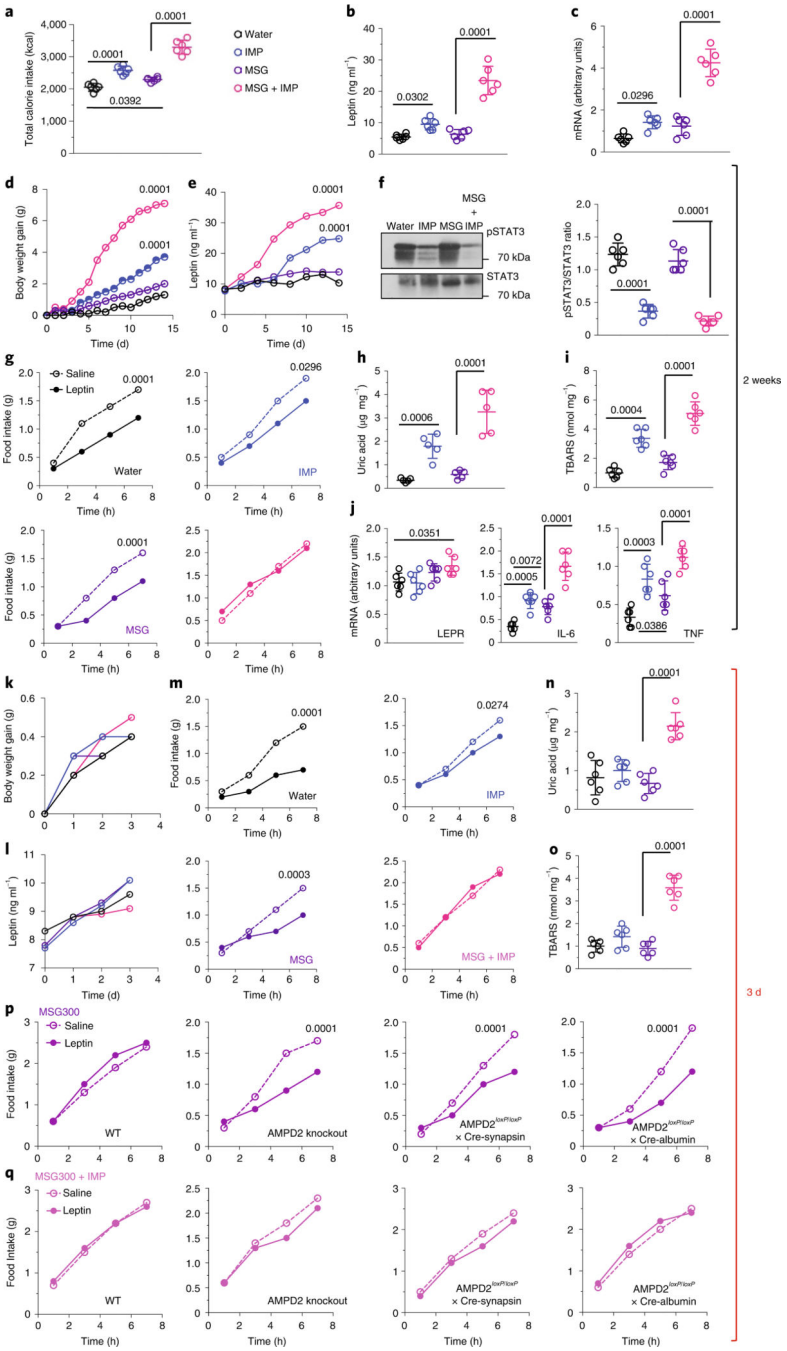

Fig. 7 |. MSG + IMP combination reduces leptin sensitivity in mice.

a, Total caloric intake of WT mice on water control or exposed to IMP (300 μM), MSG (30 mM) or an MSG + IMP combination for 30 weeks. **b**,**c**, Fasting plasma leptin (**b**) and epididymal adipose (**c**) leptin mRNA levels in WT mice of the same groups as in **a**. **d**,**e**, Body weight gain (**d**) and plasma leptin levels (**e**) over the two-week period in WT mice of the same groups as in **a**. **f**, Representative western blot and densitometry against total and active/phosphorylated hypothalamic STAT3 of mice on water control or exposed to IMP (300 μM), MSG (30 mM) or an MSG + IMP combination for 2 weeks and injected with

leptin. **g**, Seven-hour food intake after leptin injection in mice on water control or exposed to IMP (300 μM), MSG (30 mM) or an MSG + IMP combination for 2 weeks and injected with leptin. **h**,**i**, Hypothalamic uric acid (**h**) and TBARS (**i**) levels in mice on water control or exposed to IMP (300 μM), MSG (30 mM) or an MSG + IMP combination for 2 weeks. **j**, Hypothalamic mRNA levels of LEPR and the cytokines IL-6 and TNF in the same mice as in **g**. **k**,**l**, Body weight gain (**k**) and plasma leptin levels (**l**) over a 3-d period in WT mice of the same groups as in **a**. **m**, Seven-hour food intake after leptin injection in mice on water control or exposed to IMP (300 μM), MSG (30 mM) or an MSG + IMP combination for 3 d and injected with leptin. **n**,**o**, Hypothalamic uric acid (**n**) and TBAR (**o**) levels in mice on water control or exposed to IMP (300 μM), MSG (30 mM) or an MSG + IMP combination for 3 d. **p**,**q**, Seven-hour food intake after leptin injection in WT, whole-body AMPD2 knockout and neuron mice or hepatocyte-specific AMPD2 knockout mice on MSG (300 mM) (**p**) or an MSG + IMP combination for 3 d and injected with leptin (**q**). **b**,**c**,**f**,**h**–**j**,**n**,**o**, Data represent individual points with the mean ± s.e.m. **a**, Data represent the mean ± s.e.m. **d**,**e**,**g**,**k**–**m**,p,**q**, Data represent the mean. **a**–**c**,**f**,**h**–**j**,**n**,**o** One-way ANOVA. **d**,**e**,**g**,**k**–**m**,**p**,**q**, Two-tailed *t*-test. $n = 6$ mice per group.

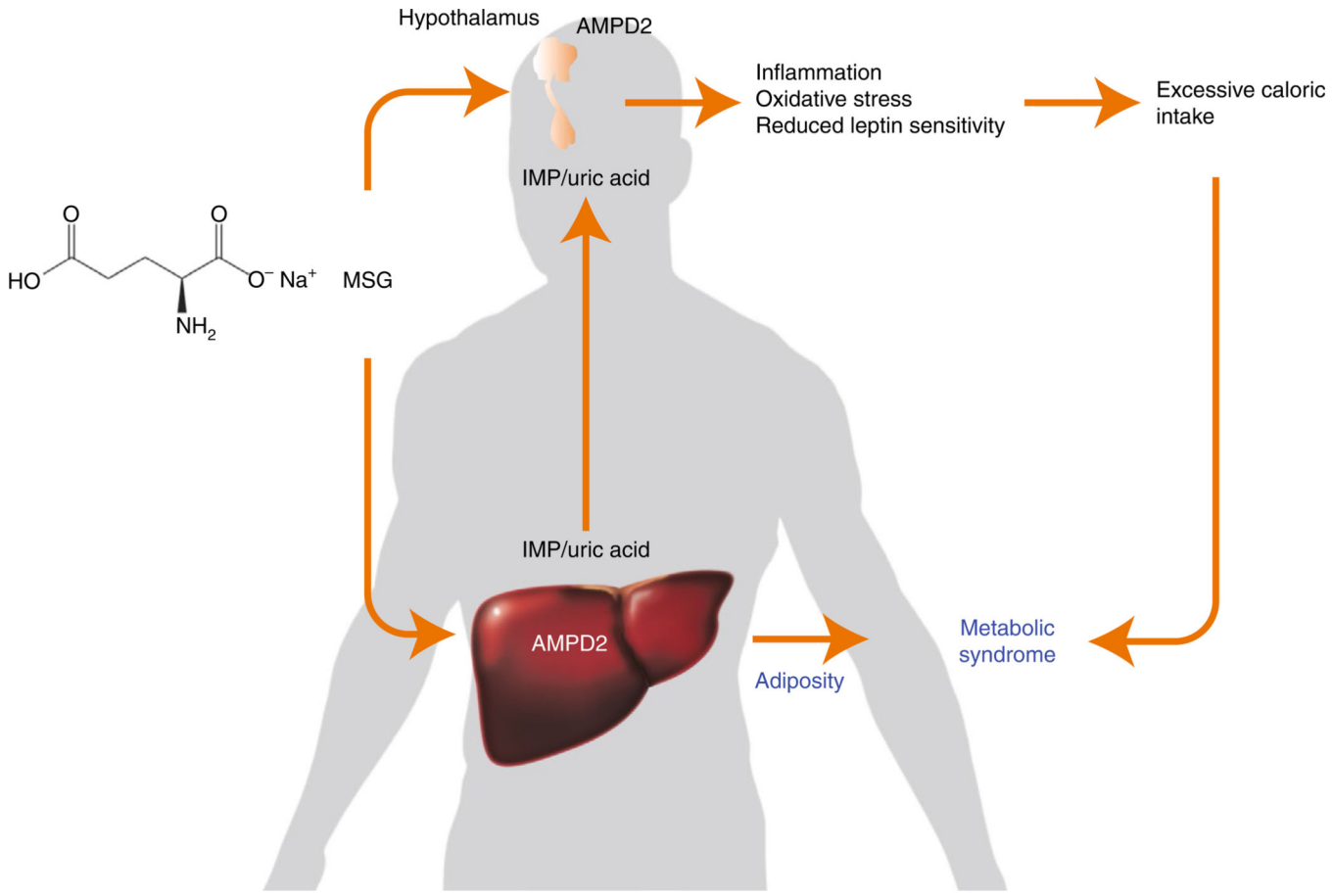

Fig. 8 |. Proposed mechanism for MSG-induced metabolic syndrome.

The addition of purines to MSG markedly exacerbates the intake of glutamate. Excessive glutamate is metabolized in the liver and hypothalamus to glutamine and ultimately IMP via the purine pathway with consumption of ATP and formation of AMP. IMP formed from both glutamine and AMP via AMPD2 enters the purine degradation pathway to generate uric acid and consequently oxidative stress and inflammation. Activation of AMPD2 in the liver drives metabolic dysfunction and adiposity while providing uric acid and IMP. Activation of AMPD2 in neurons induces inflammation and oxidative stress and reduces the sensitivity of hypothalamic neurons to leptin causing hyperphagia. Increased caloric intake and the promotion of metabolic dysfunction are the underlying factors whereby MSG and purines may cause metabolic syndrome.